Hindawi Publishing Corporation
Journal of Nanomaterials
Volume 2012, Article ID 905157, 19 pages
doi:10.1155/2012/905157

Review Article

3D Self-Supported Nanoarchitectured Arrays Electrodes for Lithium-Ion Batteries

Xin Chen,[1] Ying Du,[1,2] Nai Qing Zhang,[2,3] and Ke Ning Sun[2,3]

[1] *Department of Chemistry, Harbin Institute of Technology, Harbin, Heilongjang 150001, China*
[2] *Academy of Fundamental and Interdisciplinary Sciences, Harbin Institute of Technology, Harbin, Heilongjang 150001, China*
[3] *State Key Laboratory of Urban Water Resource and Environment, Harbin Institute of Technology, Harbin, Heilongjang 150001, China*

Correspondence should be addressed to Ke Ning Sun, keningsun@yahoo.com.cn

Received 17 October 2012; Accepted 3 December 2012

Academic Editor: Jianmin Ma

Three-dimensional self-supported nanoarchitectured arrays electrodes (3DSNAEs) consisting of a direct growth of nanoarchitectured arrays on the conductive current collector, including homogeneous and heterogeneous nanoarchitectured arrays structures, have been currently studied as the most promising electrodes owing to their synergies resulting from the multistructure hybrid and integrating heterocomponents to address the requirements (high energy and power density) of superperformance lithium ion batteries (LIBs) applied in portable electronic consumer devices, electric vehicles, large-scale electricity storage, and so on. In the paper, recent advances in the strategies for the fabrication, selection of the different current collector substrates, and structural configuration of 3DSNAEs with different cathode and anode materials are investigated in detail. The intrinsic relationship of the unique structural characters, the conductive substrates, and electrochemical kinetic properties of 3DSNAEs is minutely analyzed. Finally, the future design trends and directions of 3DSNAEs are highlighted, which may open a new avenue of developing ideal multifunctional 3DSNAEs for further advanced LIBs.

1. Introduction

Currently, extensive concern about the increasingly worsened environmental pollution and impending exhaustion of limited energy resources has brought about the ever-going demand for seeking renewable and clean energy sources to cope with these serious energy and environmental issues [1–3]. As a suitable energy source, lithium ion batteries (LIBs) are being exploited for the widespread applications [4–7] in portable electronic consumer devices, electric vehicles, and large-scale electricity storage in intelligent grids, due to the multiple superiorities such as high energy density, safety, long life, low cost, and environmental benignity.

A typical commercial LIB consists of a positive electrode (cathode) formed from layered $LiCoO_2$, a nonaqueous liquid electrolyte, and a graphite negative electrode (anode) in Figure 1(a). During the charging process, lithium ion (Li^+) is deintercalated from the layered $LiCoO_2$ host, passes through the electrolyte, and is intercalated between the graphite layers. Vice versa, discharge reverses this process. The electrons, of course, pass across the external circuit [8]. To realize the charge and discharge, the commercial LIBs are commonly constructed by electrodes and the electrolyte trapped within a polypropylene separator, in which electrodes are fabricated by the slurry procedure involved in mixing active electrodes materials with conducting carbon and polymeric binders and then casting them onto the current collector in Figure 1(b).

The electrodes materials are rated on the basis of their specific (gravimetric) capacity ($mAh\,g^{-1}$), determined by their charge/discharge graphs, and the degree of capacity change upon cycling at different demands. Intense scrutinized cathode materials, mainly including $LiCoO_2$, $LiMn_2O_4$, $LiNi_xMn_yCo_zO_2$, $LiFePO_4$, and V_2O_5 [9–13], have their own unique structured merits, offering highly accessible Li^+ diffusion pathways and demerits like limited specific capacities as well as poor capacity retention [14, 15]. Anode materials, such as carbon, silicon, alloy, metal oxides,

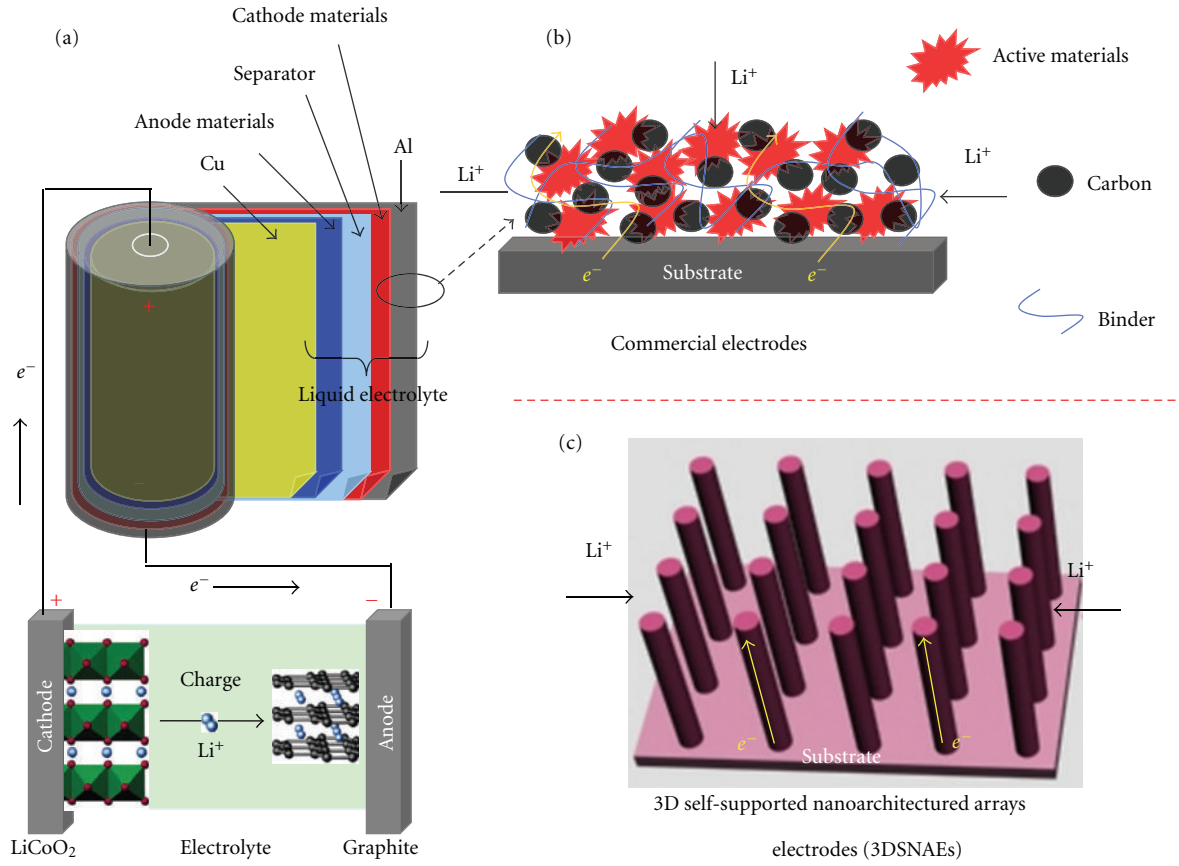

FIGURE 1: Schematic showing (a) operating principles and components of the typical commercial cylindrical lithium ion batteries (LIBs), (b) the slurry procedure of fabricating commercial electrodes, and (c) the configuration of novel 3D self-supported nanoarchitectured arrays electrodes (3DSNAEs).

and metal sulfides/phosphides, exhibit high capacities and couple to the poorly structured stability and volume variation issues [16–24]. No matter how creative researchers design new lithium intercalation materials, one drawback exists due to the intrinsic diffusivity of Li^+ in the solid state (ca. 10^{-8} cm^2 s^{-1}), which unavoidably limits the charge/discharge performance [25]. In this regard, many efforts have been devoted to devise a variety of nanomaterials with unique structures from zero-dimensional nanoparticles and one-dimensional (1D) nanowires to three-dimensional (3D) micro-/nanostructures and hollow- and core-shell structures, resulting in improved electrochemical performance to satisfy the demands of industrial applications [25–31].

These nanomaterials aforementioned have great superiorities [1, 32, 33] over their bulk counterparts. The reduced dimensions of materials shorten the Li^+ and electron transport length, leading to higher capacity at high rates. Meanwhile, a high surface area allows a large contact interface between the electrode material and electrolyte and enhances the Li^+ flux across the interface, resulting in a higher capacity. In addition, the small size could accommodate the strain associated with intercalation, reducing the capacity losses. However, nanomaterials are not a panacea to a certain extent and have some disadvantages [34, 35] such as more side reactions with the electrolyte due to the high electrolyte/electrode surface area, weak structure stabilities induced by aggregations, and lower volumetric energy density compared with microscale materials.

To transcend the above limitations of nanomaterials, selecting a proper approach, a proper structure, and a proper combination of various materials to assemble the active materials into the desired structures is indispensable. Recently, a novel configuration of 3D self-supported nanoarchitectured arrays electrodes (3DSNAEs) in Figure 1(c) has attracted much attention owing to the combination of diversified nanostructures' merits, including high surface in favor of high capacity, ordered and stable structures to the benefit of buffering for the volume change and improving the electric conductivity of electrodes, and lower aggregation and collapse in comparison to nanoparticles [36–38]. This kind of 3DSNAEs consists of a direct growth of nanoarchitectured arrays on the conductive current collector, providing a direct pathway for efficient charge transport along the arrays axis and forming a 3D conductive network among active materials, nanoarchitectured arrays pathways, and the conductive current collector. Differencing from the traditional slurry procedure, each nanoarchitectured array of 3DSNAEs is directly connected to the current-carrying substrate without any conductive and binder agents and allows for all

structures' contribution to the capacity and efficient charge transport, leading to the excellent electrochemical properties [37, 39, 40].

In this paper, detailed investigations are focused on strategies for the fabrication, selection of the different current collector substrates, and structural configuration of 3DSNAEs with different cathode and anode materials for LIBs. The intrinsic relationship of the unique structural characters, the conductive substrates, and electrochemical kinetic properties of 3DSNAEs is minutely analyzed, and recent work by our group is also summarized. Finally, the problems and prospects are highlighted on this kind of 3DSNAEs.

2. Strategies for Fabrication

Nanoarchitectured arrays of 3DSNAEs, including 1D nanowires (NWs), and nanotubes (NTs), nanorods (NRs), are apparently influenced by their properties of the conductive substrates, owing to the unique structures that nanoarchitectured arrays are directly grown on the current collector substrates. Different strategies, therefore, should be made to fabricate the 3DSNAEs grown on the different substrates. To the best of our knowledge, the conductive substrates applied in the 3DSNAEs principally contain Al, Cu, Ti, Ni, Au, Si, stainless steel (SS), Fe-based alloy, Sn-doped In_2O_3 (ITO), and so on. And the strategies to fabricate 3DSNAEs may be classified into 3 categories in Figure 2, namely, self-growing, wet-etching, and template-based growth.

Self-growing in Figure 2(a) is the one for fabricating the nanoarchitectured arrays directly grown on the substrates by using a variety of techniques such as vapor phase growth, hydro-/solvothermal growth, and solution-based growth. Vapor phase growth including thermal chemical vapor deposition (CVD), direct thermal evaporation [41], and pulsed-laser deposition (PLD) is a straightforward way that controls the reaction between oxygen gas and metal vapor source in the light of vapor-liquid-solid and vapor-solid mechanisms [42, 43]. CVD involves the process of growing the nanoarchitectured arrays on the substrate surface via the chemical reaction in the gas phase, which is resulted from the vapor with the element of nanoarchitectured arrays and other indispensable gases in the reactive chamber. By using the CVD approach, Si NWs [37] and V_2O_5/SnO_2 NWs [44] could be directly grown on the SS substrate, and V_2O_5 nanoribbons [45] would be also done on the Si substrate. Whilst employing the thermal evaporation technique, Si nanopillars [46] and SnO_2 NWs [47] could be orderly grown on the SS substrate. Besides, hydro-/solvothermal growth is a common method of preparing nanoarchitectured arrays grown on the metal or alloy substrate. The process involves the aqueous mixture of soluble metal salt (metal and/or metal-organic) of the precursor material and the treatment of the mixed solution in an autoclave filled under elevated temperature from 100°C to 300°C and relatively high pressure conditions >1 atm. Recently, MoO_x NRs on the Cu substrate [48], single-crystal mesoporous Co_3O_4 nanobelts [49] and α-Fe_2O_3 NRs [50] were prepared via the hydro-/solvothermal method. These approaches aforementioned, however, ordinarily require high temperature or high pressure. By comparison, the solution-based method based on a liquid-solid growth mechanism has been extensively exploited for preparing the free-standing nanoarchitectured arrays at the low temperature, which could reduce considerably the complexity and cost of fabrication [51, 52]. The process is that a piece of substrate immersed in reaction solutions generates a thin film with nanoarchitectured arrays at a low temperature <100°C for a while. For instance, the homogeneous and dense arrays of ZnO NWs grown on arbitrary substrates were produced by Greene et al. via the liquid-solid growth [53], and Li et al. prepared mesoporous Co_3O_4 NWs arrays on the Ti substrate by the ammonia-induced solution growth [54].

Self-etching in Figure 2(b) involves a pure chemical or electrochemical reaction process, in which the surface layer of the conductive substrates is corroded and converted immediately to nanoarchitectured arrays by using the reactions between solutions and the etching materials. Lately, some considerable efforts have been devoted to fabricate ordered 1D Si nanostructured arrays via a metal-assisted chemical etching approach [55, 56]. The etching process included the following aspects: (a) the oxidant was preferentially reduced on the surface of the noble metal; (b) the holes resulted from the reduction of the oxidant on the noble metal surface and were injected into the Si that was in contact with the noble metal; (c) the Si was oxidized and dissolved at the Si/metal interface by HF. Different from the Si etching, a solution-based corrosion is also to prepare nanoarchitectured arrays [57]. Immersed in alkaline solutions, the surface layers of Cu foil and Ni grid were corroded into 1D CuO arrays [58, 59] and Ni_3S_2 NW arrays [60], respectively. In addition, self-organized TiO_2 NTs arrays [61, 62] had been prepared via electrochemical anodization of Ti foils by controlling the electrolyte composition as well as the rate at which the resultant oxide was dissolved. To be excited, a novel vapor-phase corrosion strategy had been developed by our group to fabricate CuO hierarchically mesoporous nanosheet-assembled gearlike pillar arrays (HMNGPAs) and mesoporous nanosheet cluster arrays (MNCAs) [63, 64]. This strategy involved the oxidation, complexation, and thermal decomposition processes and was simple, low-cost, and broadly applicable, providing a new avenue for large-scale configuration of nanoarchitectured arrays with unique multifunctional properties.

Template-based growth, just as its name implies, is that the employed materials deposited in the template decorated on the substrate surface via a certain chemical or physical approach are transformed to nanoarchitectured arrays by removing the template membrane, as shown in Figure 2(c). The AAO membrane is the most widely used template, because of its facile preparation and the controllable uniformity pore distribution with lower ohmic drop, validating the homogeneous electrolyte flow. For example, arrays of perpendicular Cu nanopillars on the Cu foil substrate were fabricated by Taberna et al. via cathodic electrodepositing of the electrolyte with Cu^{2+} ion into the pores of AAO

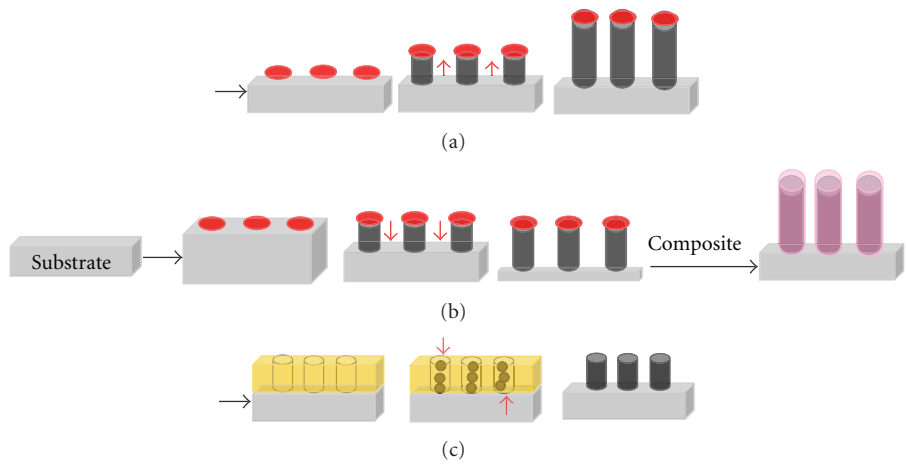

Figure 2: Schematic for the fabrication principle of 3DSNAEs by self-growing (a), self-etching (b), and template-based growth (c).

membrane [65]. Kim et al. [66] prepared vertical arrays of MnO_2 NWs on the Si substrate by the following steps: (a) sputtering a thick aluminum layer on silicon chips, (b) anodizing the aluminum layer, (c) anodic electrodepositing of MnO_2 NWs in the alumina pores, and (d) removing the AAO layer. Besides, by employing the CVD and AAO templates technique, the vertically aligned core-shell Au/CNT-V_2O_5 NRs arrays on the Al substrate had been synthesized by Kim et al. shown in Figure 3 [67]. Coupled with the previous irrigation from the top of templates, V_2O_5-TiO_2 NRs arrays were prepared by a capillary-enforced template-based method, filling into the pores of a polycarbonate membrane (PC) from the bottom with $VOSO_4$ and $TiOSO_4$ solutions [68].

3. Selecting Substrate

The current collector substrate, as a main component of 3DSNAEs, plays a significant role in the configuration and electrochemical performance of 3DSNAEs. The substrate could be classified into three major categories shown in Table 1: cathode substrate with high oxidation voltage (Al), anodic substrate with high electrochemical stability in a low voltage window (Cu), and multifunctional substrate, on the basis of functions of 3DSNAEs for LIBs.

3.1. Cathode Substrate. Generally, cathode substrate used to load cathode materials ($LiCoO_2$, $LiMn_2O_4$, and $LiFePO_4$) requires high oxidation voltage and high electrochemical stability in a wide voltage window. Al with multiple superiorities, such as high oxidation voltage (5 V versus Li/Li^+), good electric conductivity, and low price, could be protected by a thin and dense Al_2O_3 layer. However, in a low voltage close to 0 V (versus Li/Li^+), an Li-Al alloying process would happen because of the deposition of dissolved Al^{3+} from the Al_2O_3 layer of the Al foil [114, 115]. Therefore, Al is mainly used as the current collector of cathode materials for LIBs. The single-crystal V_2O_5 NRs and NTs arrays directly connected to the planar Al substrate were fabricated by Wang et al. via template-based electrodeposition and delivered 5 and 1.3 times higher capacity than sol-gel-derived films at the same current density, respectively [69, 116, 117]. Despite the improved electrochemical performance of V_2O_5 nanoarchitectured arrays, the planar Al substrate has limited surface area to provide the limited contact between active materials and substrate. In this regard, Ni NRs arrays were firstly grown on the planar Al substrate and then coated with V_2O_5 to synthesize Ni-$V_2O_5 \cdot nH_2O$ nanocable arrays, which delivered approximately 10 times higher capacities single-crystal V_2O_5 NRs and 20 times higher than sol-gel-derived V_2O_5 films, due to the large surface and short diffusion path offered by the Ni-$V_2O_5 \cdot nH_2O$ nanocable arrays [118]. Afterwards, Al NRs arrays directly grown on the Al foil to construct 3D current collectors for LIBs offered high surface area and facilitated the contribution to the capacity of active materials [119, 120]. For example, a vertically aligned Au/CNT-V_2O_5 core-shell NRs electrode developed by Kim et al. demonstrated high capacity (473.7 mAh g^{-1} at 1C rate) and excellent rate performance (379.2 mAh g^{-1} at 10C rate) owing to the aligned nanostructures with increased reaction sites, facilitated charge transport, and improved mechanical stability [67].

3.2. Anode Substrate. Cu foil has been extensively used as the current collector of anode materials, because metal Cu with good conductivity hardly forms the Li-Cu alloy at a low voltage and could be oxidized and dissolved at the high voltage (>3.6 V versus Li/Li^+) [115]. Nickel nanocones arrays (NCAs) which supported Si anode was firstly constructed by Zhang et al. via the electrodepositing and sputtering techniques and delivered a high capacity of 2400 mAh g^{-1} at 0.2C rate over 100 cycles, because Ni NCAs facilitated charge collection and transport, supported the electrode structure, and acted as inactive confining buffers [121]. Thanks to factors that the chemical property of metal Cu is considerably brisk and easy to be corroded by acid or alkali solutions. The template-based growth is an effective strategy to construct 3DSNAEs on the Cu substrate.

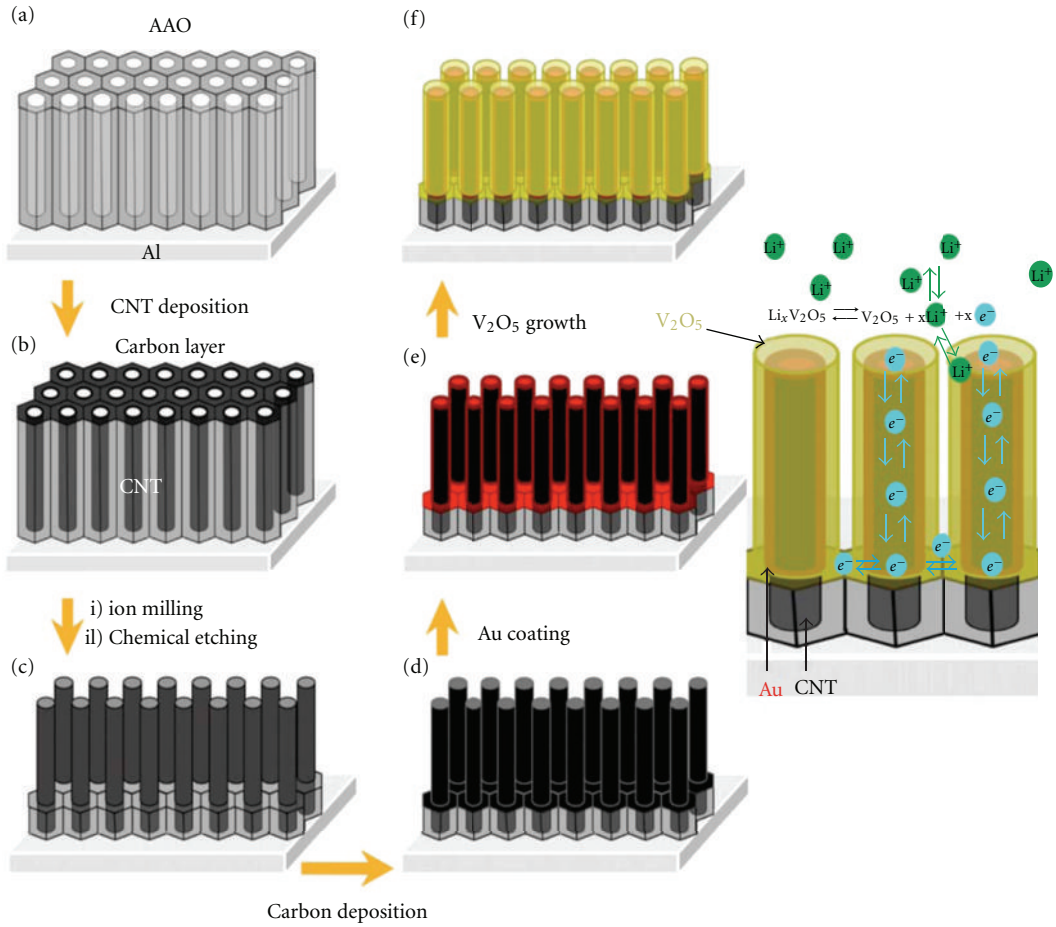

FIGURE 3: Schematic of the fabrication process of Au/CNT-V_2O_5 core-shell nanorod arrays with the schematized electrochemical reaction involving the nanostructured Li battery electrode [67].

Since Taberna et al. prepared Cu NRs arrays on the Cu substrate to construct Cu NRs arrays supported Fe_3O_4 via AAO template-based electrodeposition [65], many anode materials such as Cu-Fe_3O_4 [122, 123], Cu-Sn [74, 124], Cu-Bi [75], Cu-Cu_3P [84], and Cu-Ni_3Sn_4 [18] have been developed by the template-based growth. For example, as the anode materials, Cu-Ni_3Sn_4 delivered a capacity of 500 mAh g^{-1} with no decay over 200 cycles at 0.8*C* rate. In addition, solution-based growth is also an efficient way to large-scale fabricateion of 3DSNAEs on the Cu substrate, due to the easy realization of the preparation conditions. By varying these parameters including the ratio of reaction precursor ions, temperature, and immersing time, CuO NTs [58], nanobelts [59], NRs [76], ZnO NRs [77], and Cu_2S NWs [83] could be directly grown on the Cu substrate. At 0.5*C* rate, CuO NRs delivered a high capacity of 650 mAh g^{-1} with no capacity decay even after 100 cycles. Even at a high rate as high as 20*C*, Cu_2S NWs were capable of delivering a reversible capacity of 145 mAh g^{-1}.

Metal Ni is widely available in many forms, such as foil, grid, and felts, and is stable up to 4.5 V (versus Li/Li^+), after which the electrodissolution of Ni begins [125]. Ni is commonly used as the current collector of anode materials. Fan et al. reported that freestanding Co_3O_4 nanosheets on the Ni foil substrate delivered a reversible capacity of 631 mAh g^{-1} after 50 cycles at a constant current of 150 mA g^{-1} in a fixed voltage window from 2.5 V to 0.01 V [87]. Wu et al. prepared interconnected MnO_2 NWs on the Ni foil substrate by electrodeposition, which delivered reversible capacity of 800 mAh g^{-1} and with low capacity decay after 100 cycles [86]. Additionally, the oriented Ni_3S_2 NWs arrays on the Ni grid substrate fabricated via the solution-based growth showed a reversible capacity of 430 mAh g^{-1} with the capacity retention 80% over 100 cycles [60].

Fe is an inexpensive metal and cannot generate Li-Fe alloy at 0 V (versus Li/Li^+) during polarization in the cathodic direction; thus, Fe-based alloy substrate could be exploited for loading the metal oxide anode materials to construct 3DSNAEs via the hydro-/solvothermal growth. By controlling the conditions of the hydro-/solvothermal growth, Liu and coworkers have prepared SnO_2 NRs [88], C/α-Fe_2O_3 NTs [89], ZnO/C NRs [90], and SnO_2/C NRs [126] directly grown on the Fe-base alloy substrate. The C/α-Fe_2O_3 NTs retained a reversible capacity of as high as 659 mAh g^{-1} at 0.2*C* rate after 150 cycles, and the pristine α-Fe_2O_3 NTs maintained only 384 mAh g^{-1} at the same conditions. Such good electrochemical performance may be attributed to the nanoscale intimate contact of α-Fe_2O_3 with

Table 1: A summary of optimizing various electrode materials and suitable strategies to construct 3DSNAEs on various current collector substrates.

3DSANEs	Collector	Materials	Growth method	Remark
Cathode	Al	V_2O_5 [69], $LiCoO_2$ [70]	Template-based chemical or physical deposition	Needing complicated synthesis techniques
	Sn-doped In_2O_3 (ITO)	V_2O_5-TiO_2 [68], $InVO_4$ [71]	Chemical or physical deposition	
Anode	Cu	CNTs [72], Si [73], metal (Sn, Bi) [74, 75], MO (M = Fe, Cu, Zn, Ni) [65, 76–78], alloy (SnCo [79], NiSn [18, 80, 81], SiGe [82]), Cu_2S [83], Cu_3P [84], Sn/graphene [85]	Template-based chemical or physical deposition	It is a technique for large scale preparation
			Solution-based growth	
	Ni	Ni_3S_2 [60], MnO_2 [86], Co_3O_4 [87]	Electrodeposition, solution-based growth	
	Fe-based alloy	MO (M = Sn, Fe, Zn) [88–90]	Hydrothermal, solution-based growth	
Cathode or anode	Gold	SnO_2 [91], CNT-MnO_2 [92], SnCo [93]	Template-based chemical or physical deposition	Needing complicated synthesis techniques
	The stainless steel	CNTs [94], Ge [95], Si [37, 96–99], CNT-Si [100], Si/Cu [101], SnO_2 [47], ITO/TiO_2 [102], Ni/MnO_2 [103], Fe_2O_3/SnO_2 [104], V_2O_5/SnO_2 [44], CNTs-$LiCoO_2$ ($LiMn_2O_4$) [105], CNTs-$LiCoPO_4$ [106, 107]	Chemical/physical vapor deposition	Needing high temperature
	Ti	V_2O_5 [108], MO (M = Ti, Co, Fe, Sn) [49, 50, 62, 109]	Anodization, hydro/solvothermal, Solution-based growth	It is a hope for large scale preparation
	Si	V_2O_5 [45], Si [56], Si/NiO [110], MnO_2 [111], Cu_2O [112], Sn [113]	Chemical/physical deposition, etching	Needing complicated synthesis techniques

conductive carbon framework and the unique porous tubular nanostructures readily derived from sacrificial template-accelerated hydrolysis.

3.3. Dual Functional Substrate. Dual functional substrate, including SS, Ti, Ni, and Si, could act as cathode or anode substrate, owing to the superiorities such as a high oxidation voltage and non-Li-metal alloying process in a low voltage.

As an inert substrate, SS with a high oxidation voltage (5 V versus Li/Li^+) has been widely used as the current collector for LIBs, because the Cr and Fe oxides on the surface protect the metal bulk from general corrosion. To the best of our knowledge, CVD and physical vapor deposition (PVD) are usually developed to construct 3DSNAEs on the SS substrate. Masarapu et al. found that aligned multiwall carbon nanotubes (MWNTs) on the SS substrate obtained by CVD technique delivered an initial capacity of 132 mAh g^{-1} at 1*C* rate and a reversible capacity of 460 mAh g^{-1} after 1200 cycles, attributing to the morphology of the MWNTs with structural and surface defects and the SS substrate' contribution to capacity [94]. Chan and coworkers prepared a series of Si-based nanoarchitectured arrays on the SS substrate by using CVD [37, 72, 95, 97] and found that Si NWs exhibited a stable capacity ~3500 mAh g^{-1} for 20 cycles. Besides, Yan et al. used multistep CVD to construct V_2O_5/SnO_2 NWs with high power density of 60 kW kg^{-1} and energy density of as high as 282 Wh kg^{-1} [44]. Such excellent performance might be ascribed to the unique core/shell structure that the thin V_2O_5 layer was in favor of the fast Li^+ lithiation/delithiation, and the SnO_2 core offered a fast path for electron transportation and also increased the utilization of V_2O_5. By employing PVD technique, the vertical Si nanopillars arrays and single-crystal SnO_2 NWs on the SS substrate were also fabricated by Fleischauer et al. [46] and Ko et al. [47]. The SnO_2 NWs delivered a high discharge capacity of 510 mAh g^{-1} after 50 cycles at 1*C* rate and displayed superior rate capability of 440 mAh g^{-1} at 10*C* rate.

Metal Ti is very resistive to the alkaline ammonia solution and oxidation, does not alloy with lithium at low voltage, and therefore is a good current collector material for LIBs [127]. V_2O_5 nanobelt arrays on the Ti substrate prepared via hydrothermal growth could deliver a reversible capacity of 240 mAh g^{-1} stably after 50 cycles at the current density of 400 mA g^{-1}, and a high rate capacity of 150 mAh g^{-1} at 4000 mA g^{-1} [108]. And the mesoporous Co_3O_4 NWs arrays on the Ti substrate via solution-based growth exhibited a high reversible capacity of 859 mAh g^{-1} at the current density of 111 mA g^{-1} and high rate capacities of 450 mAh g^{-1} at 2220 mA g^{-1} and 240 mAh g^{-1} at 5550 mA g^{-1} [54]. Whilst directly anodizing and annealing Ti foil, the self-organized TiO_2 NTs on the Ti substrate could be obtained. Ortiz et al. found that the amorphous TiO_2 NTs delivered a highest capacity of 77 μAh cm^{-2}, and crystalline TiO_2 NTs had the best capacity retention up to 90% over 50 cycles [62]. Wei et al. reported that the TiO_2 NTs with 50 nm pore size and 20 nm thickness showed the highest reversible capacity of

180 mAh g^{-1} over 140 cycles [128]. Liu and coworkers found that TiO_2 NTs annealed at N_2 possessed an initial discharge capacity of 163 mAh g^{-1} and maintained 145 mAh g^{-1} over 50 cycles and that TiO_2 NTs annealed at CO exhibited an initial capacity of 223 mAh g^{-1} with the reversible capacity of 179 mAh g^{-1} at the 50th cycle [129, 130]. The results might be attributed to the presence of surface defects like Ti-C species and Ti^{3+} groups with oxygen vacancies, improving the charge-transfer conductivity of the arrays and promoting phase transition.

Although Si could form Li-Si alloy at ca. 0.12 V (versus Li/Li^+), crystalline Si cores of core-shell crystal-amorphous Si NWs functioned as not active material store but a stable mechanical support [97]. Therefore, the Si substrate can act as a dual functional substrate for loading cathode or anode materials to construct 3DSNAEs. Chan et al. prepared single-crystal V_2O_5 nanoribbons via thermal vapor deposition and found that transformation of V_2O_5 into the ω-$Li_3V_2O_5$ phase could take place within 10 s in thin nanoribbons, suggesting a significant increase in battery power density [45]. Liu and coworkers found that $MnO_2 \cdot 0.5H_2O$ nanowall arrays electrodeposited on the Si substrate exhibited a reversible capacity of 220 mAh g^{-1} over 50 cycles at 0.5*C* rate and mesoporous $MnO_2 \cdot 0.5H_2O$ nanowall arrays with 500 nm thickness delivered a stable capacity of 256 mAh g^{-1} [111, 131]. Such excellent electrochemical performance might be ascribed to the hierarchically structured macro- and mesoporosity of $MnO_2 \cdot 0.5H_2O$, which offered a large surface area to volume ratio of favoring interface faradic reactions and shortened solid-state diffusion paths. Moreover, Kim et al. prepared vertical arrays of Sn NWs on the Si substrate via AAO template-based electrodeposition [113], which showed the discharge capacity of 400 mAh g^{-1} after 15 cycles at the current density of 4200 mA g^{-1}.

4. Structural Configuration

As electrodes materials of LIBs, nanomaterials could enhance charge/discharge kinetics and improve high Li storage capacity, despite of suffering from low thermodynamic stability and surface side-reactions. Optimizing and designing proper nanoarchitectured arrays to take advantages and restrain disadvantages of electrodes materials are, therefore, of particular importance to the electrochemical properties of 3DSNAEs. Types of the 3DSNAEs structure reviewed here contain homogeneous nanoarchitectured arrays and heterogeneous nanoarchitectured arrays (Figure 4).

4.1. Homogenous Nanoarchitectured Arrays. Homogenous nanoarchitectured arrays, namely, single-component nanostructure arrays, mainly include simple nanostructure arrays, nanostructure cluster arrays, and nanostructure gearlike arrays on the basis of the structure characteristic of nanoarchitectured arrays. For this category, nanostructure arrays directly connected to the conductive substrate are used as both the structural support and electroactive materials to alleviate large strain without pulverization and provide good electronic contact and conduction. Electroactive materials of nanoarchitectured arrays, therefore, are considerably rigorous and should possess the merits including a degree of conductivity and easy growth controll.

Simple nanostructure arrays are commonly composed of single-phase 1D NWs, NTs, and NRs arrays directly connected to the conductive substrate. Up to now, the 1D array materials such as V_2O_5 nanobelts [108], multiwall carbon nanotubes (MWCNTs) [72, 94], Si NWs [132], Ge NWs [95], Sn NWs [113], SnO_2 NRs [88], and MnO_2 NWs [86] have been developed to act as the 3DSNAEs with rate capability and cycling stability. V_2O_5 nanobelts directly grown on a Ti substrate based on the hydrogen bonding action delivered high reversible capacity of 650 and 520 mAh g^{-1} after 50 cycles at the current density of 1.2 and 3 A g^{-1}, respectively. MWCNTs directly grown on a Cu current collector (MWCNT-on-Cu) in Figure 5 were synthesized by a two-step process of catalyst deposition and CVD and showed a high reversible capacity of 900 mAh g^{-1} after 50 cycles at 1*C* rate. Excellent electrochemical properties of MWCNT-on-Cu structure could be ascribed to high Li ion intercalation on the carbon nanotube walls, strongly bonding with the Cu substrate and good conductivity.

Nanostructure cluster arrays, generally, consist of clusters of assembled NWs, NRs, and nanosheets. Because NWs, NRs and nanosheets are usually inclined to aggregate and form the nanostructure clusters due to their structural instability. Some nanostructure cluster arrays, recently, including network-like and flower-like CuO [133, 134], CuO MNCAs [64], and CuO pine-needle-like (PNL) arrays (see Figure 6) [135], have been used as the 3DSNAEs with enhanced lithium storage properties. CuO MNCAs synthesized by our group exhibited a high reversible capacity of 639.8 mAh g^{-1} after 100 cycles at 1*C* rate and a high-rate capability of 548.8 mAh g^{-1} at 10*C* rate. CuO PNL arrays fabricated by our group via an anodic route delivered high rate capacity of 545.9 and 492.2 mAh g^{-1} at 15*C* and 20*C* rates and exhibited excellent cyclability of 583.1 mAh g^{-1} after 100 cycles at 2*C* rate. The enhanced lithium storage properties could be ascribed to the unique nanostructure cluster arrays, which provide suitable branches for lithium storage and suitable free space to facilitate Li^+ flux across the interface as well as accommodating the large volume variation.

Nanostructure gearlike arrays. In this respect, the size of arrays directly connect to the substrate is mainly microscale, which is stable and easy to controlled synthesis by a simple approach. Furthermore, microarrays are ordinarily assembled by a mass of nanosheets, NWs, or NBs with the same component, in favor of enlarging the contact areas between active materials and electrolyte. The microscale coglike CuO fabricated by the microemulsion-mediated method exhibited a high reversible capacity of 583 mAh g^{-1} at a rate of 4*C* [136]. In our work, CuO HMNGPAs [63] shown in Figure 7 have been synthesized via a novel vapor-phase corrosion strategy and exhibited excellent cycling stability of 651.6 mAh g^{-1} after 100 cycles at 0.5*C* rate and high-rate capability of 561.6 mAh g^{-1} at 10*C* rate, because the unique HMNGPAs consisting of numerous gearlike pillars assembled by nanosheets could take full advantage of both micro and nano, namely, micropillars with structural

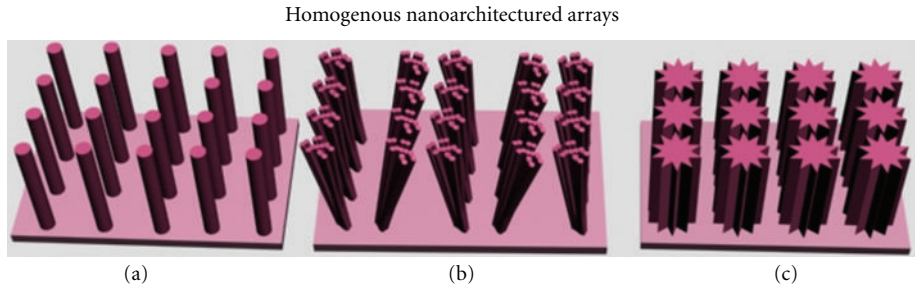

Figure 4: Schematic of homogenous nanoarchitectured arrays. (a) Simple nanostructure arrays, (b) nanostructure cluster arrays, and (c) nanostructure gearlike arrays.

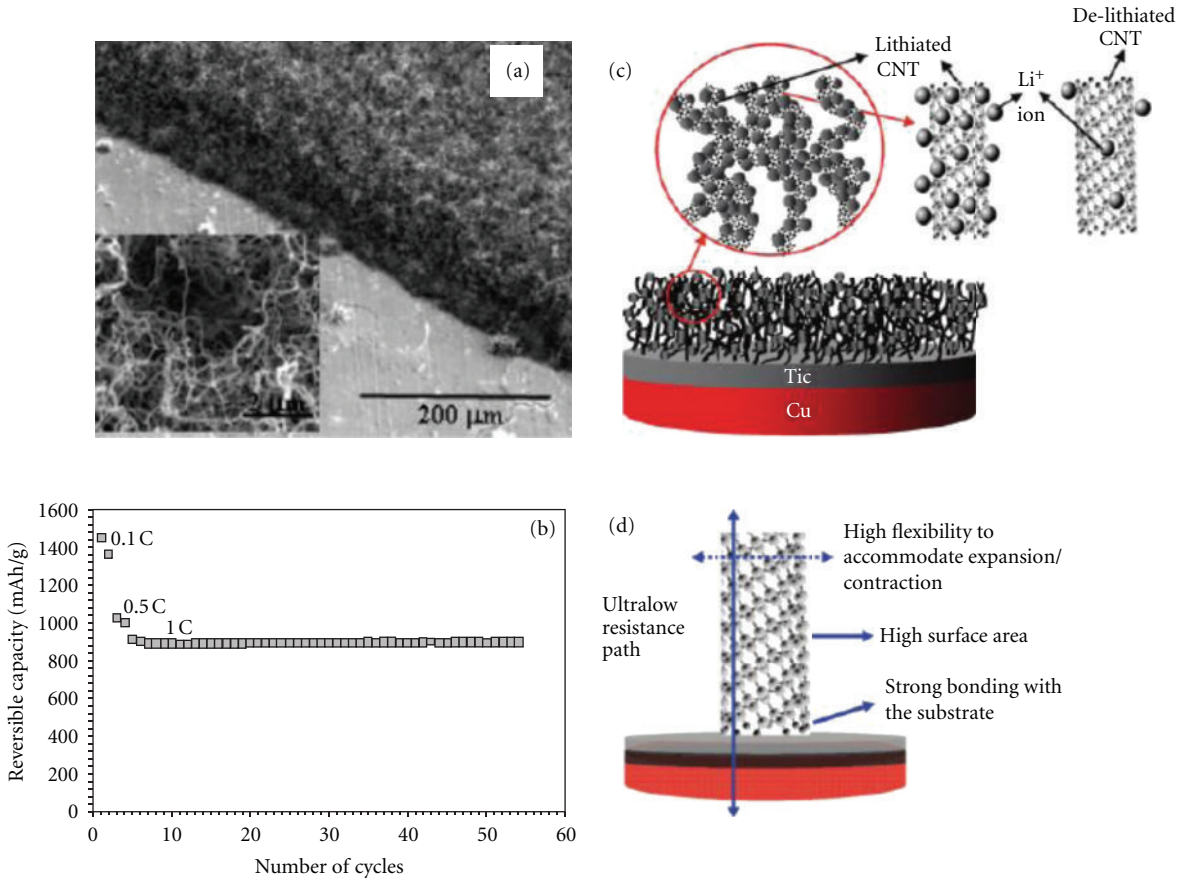

Figure 5: (a) SEM images of the as-grown MWCNT-on-Cu structure. (b) Exceptional stability of the reversible capacity of the MWCNT-on-Cu anode in long-run, at 1*C* rate. (c) A schematic of the proposed lithiation/delithiation mechanism. (d) A schematic of the proposed anode structure [72].

stability and mesoporous nanosheets with high lithium-storage sites.

4.2. Heterogeneous Nanoarchitectured Arrays. Heterogeneous nanoarchitectured array are hybrid nanostructure arrays with multinanocomponents each tailored to satisfy different demands such as high energy density, high conductivity, and excellent mechanical stability. On the basis of the structural characteristic, heterogeneous nanoarchitectured arrays could be classified to six types, including (a) simple heterogeneous nanostructure arrays, (b) coaxial or core/shell heterogeneous nanostructure arrays, (c) semicoated grenadelike heterogeneous nanostructure arrays, (d) dispersed heterogeneous nanostructure arrays, (e) branched heterogeneous nanostructure arrays, and (h) folded heterogeneous nanostructure arrays (Figure 8).

4.2.1. Simple Heterogeneous Nanostructure Arrays. Generally, this kind of structure is composed of 1D array structures with two or more components used as active materials, on the basis of the dual lithium insertion/desertion mechanism. V_2O_5-TiO_2 NRs arrays with molar ratio

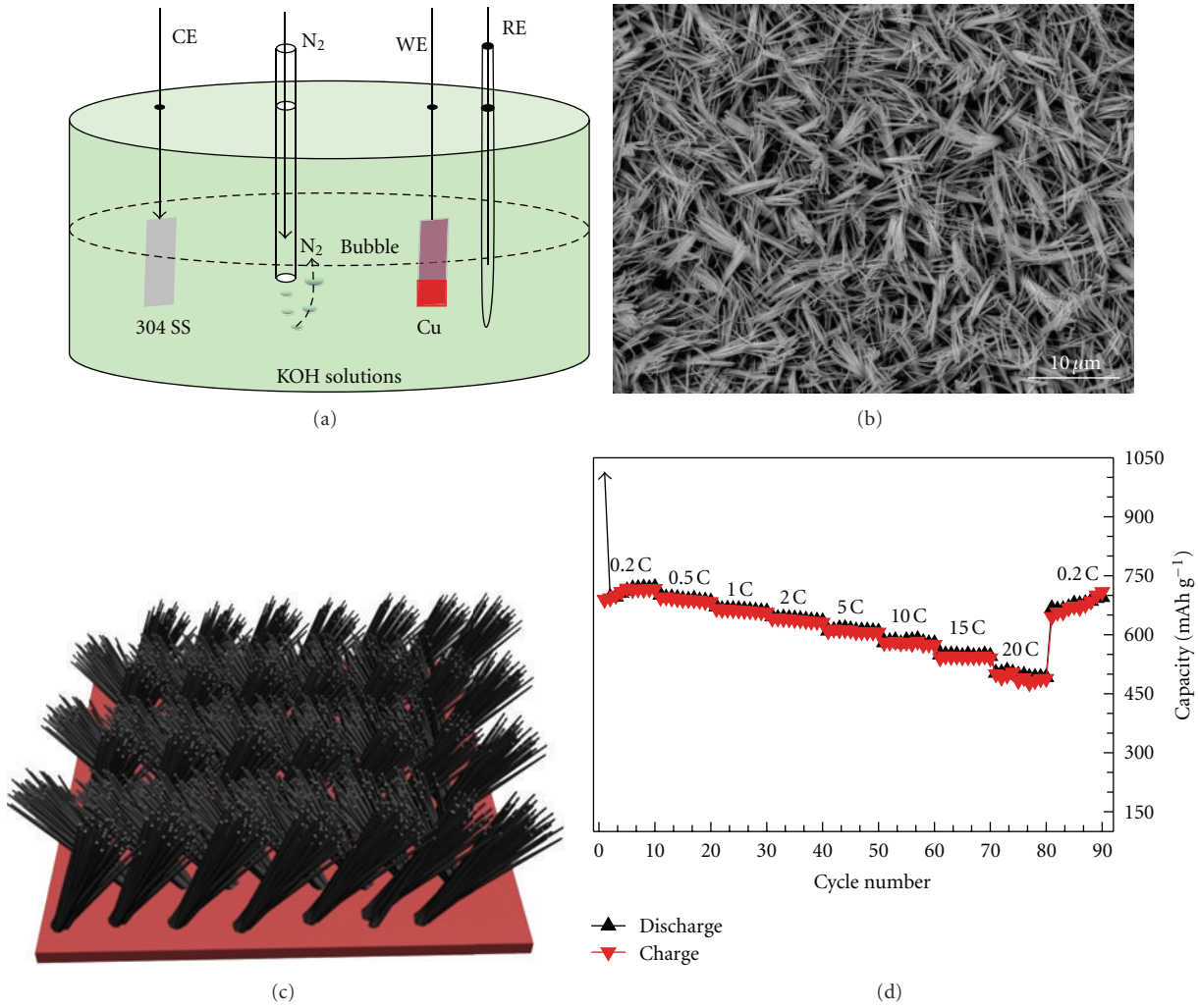

FIGURE 6: (a) A schematic of the cell used for the preparation of $Cu(OH)_2$ PNL arrays, wherein CE, WE, and RE represent the counter, working, and reference electrode, respectively. SEM image (b), structural schematic (c), and rate cyclability (d) of CuO PNL arrays gained by annealing $Cu(OH)_2$ PNL arrays [135].

V/Ti = 75/25 prepared by Takahashi et al. could deliver 1.5 times discharge capacity of V_2O_5 NRs at the current density of 92 mA g^{-1}, resulting from the change of crystallinity and interaction forces between adjacent layers in V_2O_5 [68]. SnO_2/α-Fe_2O_3 NTs arrays fabricated by Zeng et al. showed high areal capacities of 1.289 mAh cm^{-2} at a current rate of 0.1 mA cm^{-2}, possibly due to the synergistic lithium storage of SnO_2 and α-Fe_2O_3 electroactive materials [137].

4.2.2. Coaxial or Core/Shell Heterogeneous Nanostructure Arrays. In this case, the coaxial or core/shell structures refer to 1D array inner cores coated completely by other materials as shells. The functions of 1D array inner cores and shells can be both the structural support and electroactive materials on the basis of the particularity of 1D array directly connected to the conductive substrate.

While the 1D array inner cores are only used as the structural support, the outer shells are used as the electroactive materials, and the unique structured materials containing Al NRs-$LiCoO_2$ (see Figure 9) [70], Cu NRs-Fe_3O_4 [65], Cu-Si nanocable [138], Cu-$Si_{1-x}Ge_x$ NWs [82], hybrid ITO/TiO_2 [102], and Ni/Si NWs [139] exhibit a super high-rate performance. For example, the Cu-Si nanocable exhibited a specific capacity as high as 1890 mAh g^{-1} under a current density of 0.3 A g^{-1} and 1660 mAh g^{-1} under a current density of 1.4 A g^{-1}. Hybrid ITO/TiO_2 demonstrated an extremely low average capacity fading ~0.1% per cycle for 1000 cycles at a current density of 60*C*. The previous excellent lithium storage properties could be related to the unique Al, Cu, ITO, and Ni 1D nanostructures directly connected to the conductive substrate, which act as inner cores of electroactive materials and form the 3D conductive network of the current collectors, providing both efficient pathways for ion and electron transport, improving the energy density per unit area.

The other strategy is that the 1D array inner cores act as the active materials and the shell as conductive agents (amorphous carbon). The semiconductor metal oxides have been usually constructed to the core/shell Fe_2O_3/C NTs and

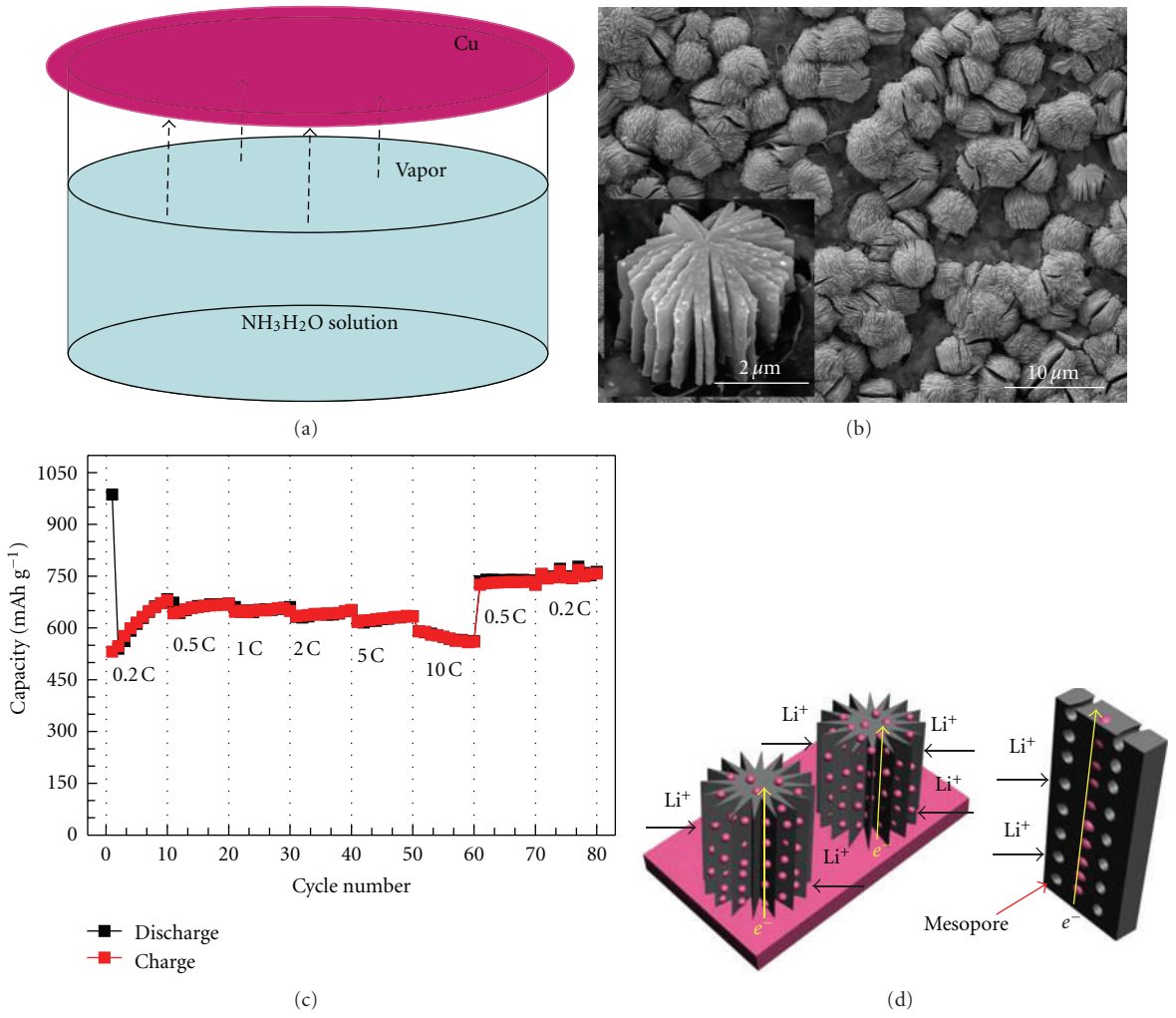

FIGURE 7: (a) Schematic device of the ammonia vapor-phase corrosion route. SEM images (b), rate cyclability (c), and a schematic diagram of discharge-charge (d) of CuO HMNGPAs [63].

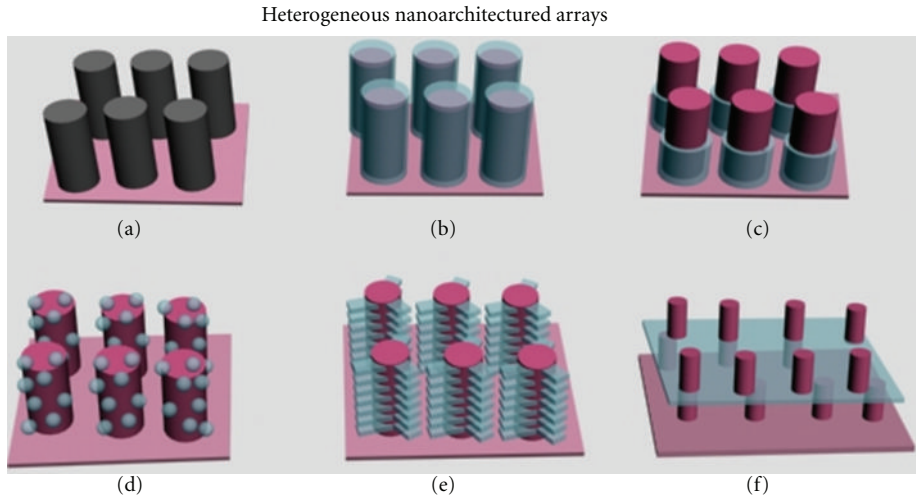

FIGURE 8: Schematic of heterogeneous nanoarchitectured arrays based on structural complexity. (a) Simple heterogeneous nanostructure arrays, (b) coaxial or core/shell heterogeneous nanostructure arrays, (c) semicoated grenadelike heterogeneous nanostructure arrays, (d) dispersed heterogeneous nanostructure arrays, (e) branched heterogeneous nanostructure arrays, and (f) folded heterogeneous nanostructure arrays.

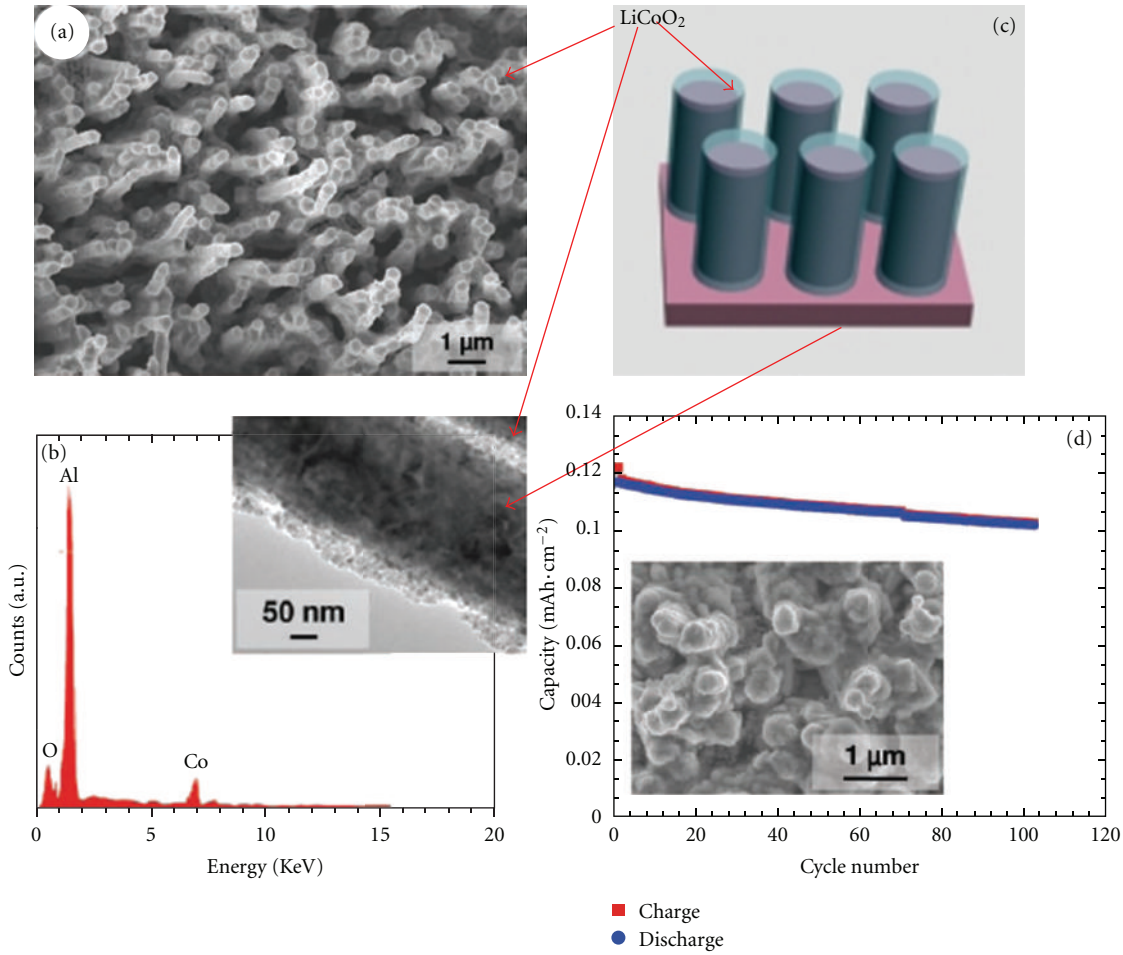

FIGURE 9: SEM images (a), EDX pattern (b), structural schematic (c), and cycling performance (d) of Al NRs-$LiCoO_2$. Insert of (b) shows a TEM image of Al NRs-$LiCoO_2$, and insert of (d) shows an SEM image of Al NRs-$LiCoO_2$ 3D electrode cycled 50 times at 0.2*C* rate [70].

NRs [50, 89], ZnO/C [90], and SnO_2/C NRs [126] arrays, wherein metal oxides functioned as both the active core and the structural skeleton, and the carbon shells (nano-Cu) are used to improve the conductivity of materials and suppress the volume expansion. SnO_2/C NRs prepared by a two-step hydrothermal method exhibited a high reversible capacity of 585 mAh g^{-1} after 50 cycles at 500 mA g^{-1}. Furthermore, a new copper-coating layer has better conductivity than carbon and can suppress electrolyte decomposition on the surface of 1D array. Chen et al. found the copper-coated Si NWs showed an initial Coulombic efficiency of 90.3% at a current density of 210 mA g^{-1} [101].

The third way is that the inner cores and shells are both the active materials to construct the coaxial SnO_2 NWs/CNTs [91], hybrid MnO_2/CNTs [92], and C-Si NTs sponge [140]. Hybrid MnO_2/CNTs delivered the first discharge capacity of 2170 mAh g^{-1} and a reversible capacity of ~500 mAh g^{-1} after 15 cycles. This kind of material showed the good charge/discharge performance, due to the dual lithium storage mechanism of insertion/desertion, in which CNTs acted as a highly conductive backbone to accommodate the volume expansion and avoid agglomeration.

4.2.3. Semicoated Grenadelike Heterogeneous Nanostructure Arrays. The grenadelike structure is analogous to the core/shell structure and composed of inner cores and outer shells. The difference, however, is that the outer shell of grenadelike structures is semicoated. Generally, the inner core is the major component with functional properties, while the outer shell acts as the structural support. Ortiz et al. prepared NWs SnO/NTs TiO_2 [141] and NWs Fe_2O_3/NTs TiO_2 (see Figure 10) [142] in the matrix of TiO_2 NTs by anodization and electrodeposition. At the current density of 50 μA cm^{-2}, NWs SnO/NTs TiO_2 exhibited a remarkable reversible capacity of about 140 μAh cm^{-2} with the capacity retention of ca. 85% over 50 cycles. The enhanced electrochemical performance could be ascribed to the TiO_2 NTs matrix that allows the volume expansion during the Li^+ insertion and desertion process.

4.2.4. Dispersed Heterogeneous Nanostructure Arrays. In this dispersed structure, nanomaterials are commonly anchored on the surface of 1D array to be used as the electroactive components or the conductive network for facile electrons transport. While the 1D array (CNTs and Si NWs)

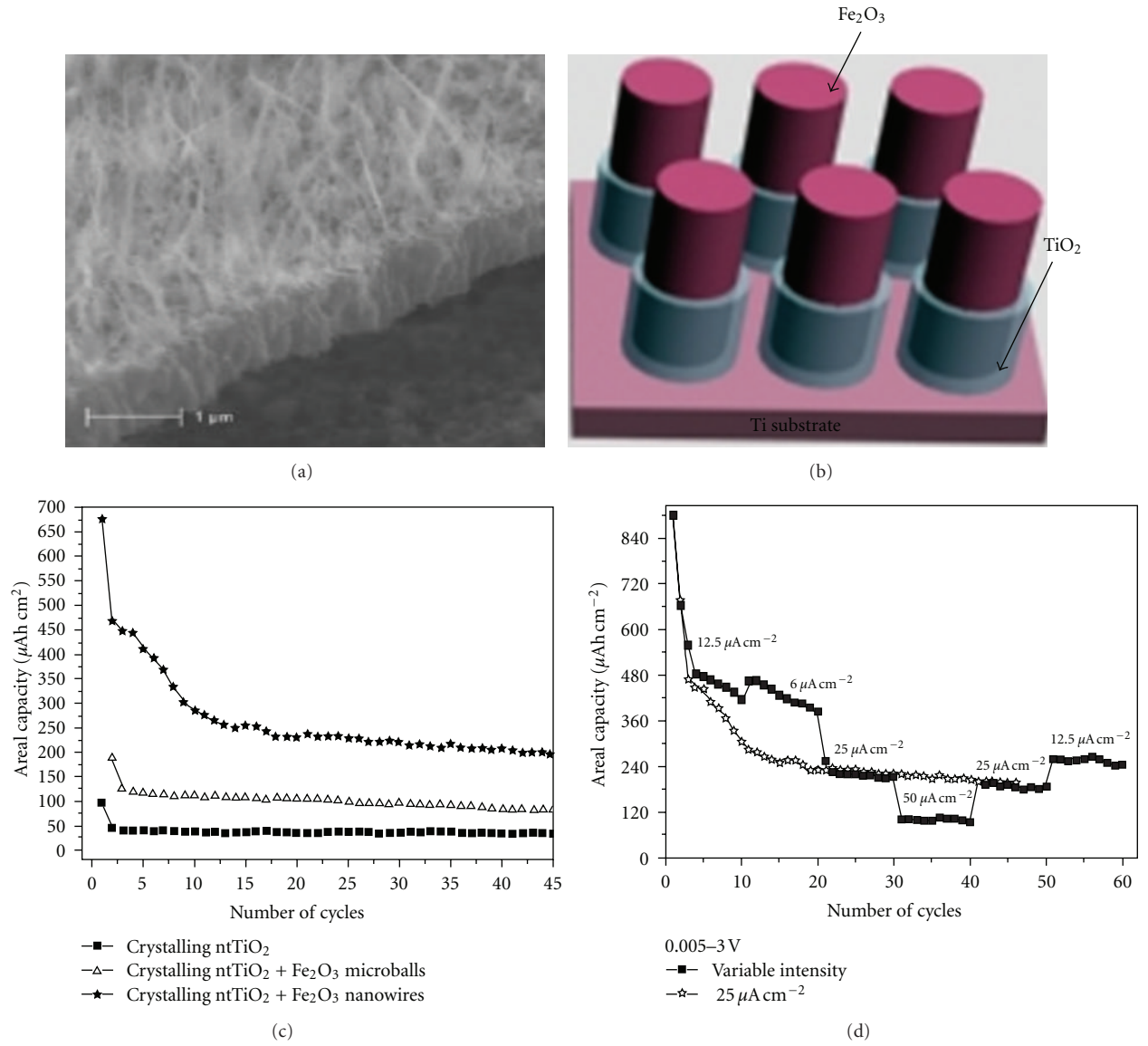

Figure 10: SEM images (a) and structural schematic (b) of nanocomposite NWs Fe_2O_3/NTs TiO_2, cycling life (c), and rate performance (d) of nanocomposite electrodes [142].

functioned as the electrical conducting pathway and the stable mechanical support for strain release, the anchored nanomaterials including $LiCoO_2$ ($LiMn_2O_4$) [105], $LiCoPO_4$ [106, 107], and NiO NWs [110] acted as the electroactive components. The binder-free $LiCoO_2$-3 wt% SACNTs composites could deliver high reversible capacities of 145.7 mAh g^{-1} at 0.1*C* rate and 130.4 mAh g^{-1} at 2C rate. The ordered NiO-coated Si NWs arrays showed a reversible capacity of 606.13 mAh g^{-1} at the rate of 50 mA g^{-1} after 30 cycles. While the dispersed nanomaterials (Ag nanoparticles) are mainly applied to improve the conductive and utilization of the active materials, the Co_3O_4-Ag NWs arrays exhibited more than 82% capacity retention at the current density of 2000 mA g^{-1} after 20 cycles, in comparison with 74% capacity retention of the pristine Co_3O_4 arrays [143]. When 1D array and dispersed nanomaterials are both used as electroactive materials, these structural materials of VA CNTs-Si [100, 144–146] showed high rate capacities of lithium storage. For instance, VA-CNTs/Si arrays shown in Figure 11 via a two-step CVD technique exhibited high discharge capacities of 2980, 1890, and 765 mAh g^{-1} at 1.3*C*, 5*C* and 15*C* rate, respectively.

4.2.5. Branched Heterogeneous Nanostructure Arrays. Being similar to core-shell structure, branched heterogeneous nanostructure arrays, generally, consist of an inner core and outer shell with a branched structure and possess both all desired functions of each component and a strong synergetic enhancement. More specifically, the inner core provides a direct pathway for electron transport, while the outer shell maintains the structural stability of the inner core during the discharge-charge process. The core-shell Ni/MnO_2 hybrid

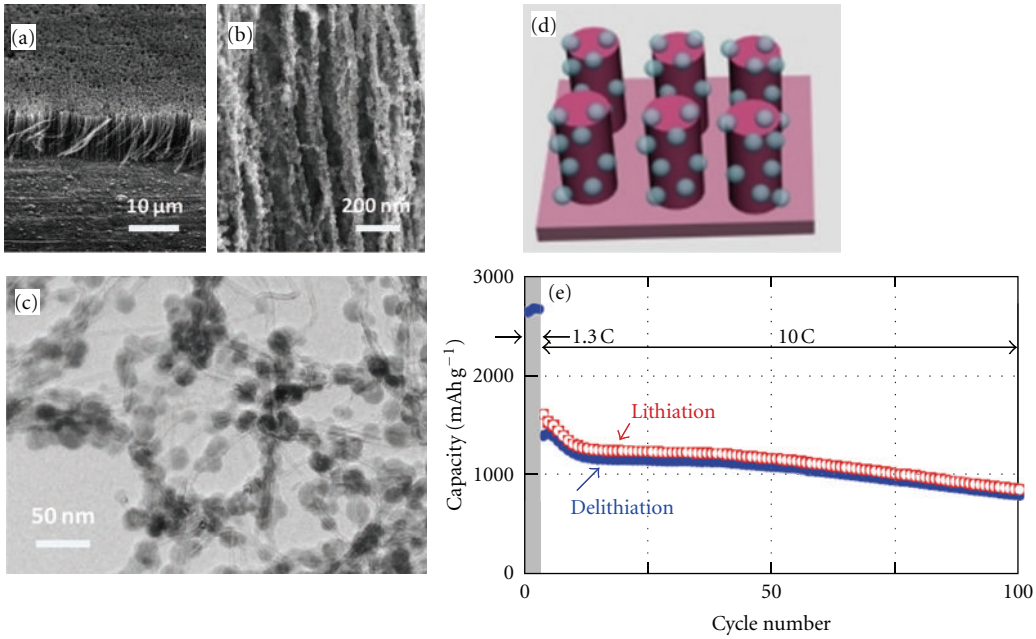

Figure 11: SEM (a, b), TEM (c) images, structural schematic (d), and cycling performance (e) of the as-prepared VA-CNTs/Si arrays on the Si substrate [146].

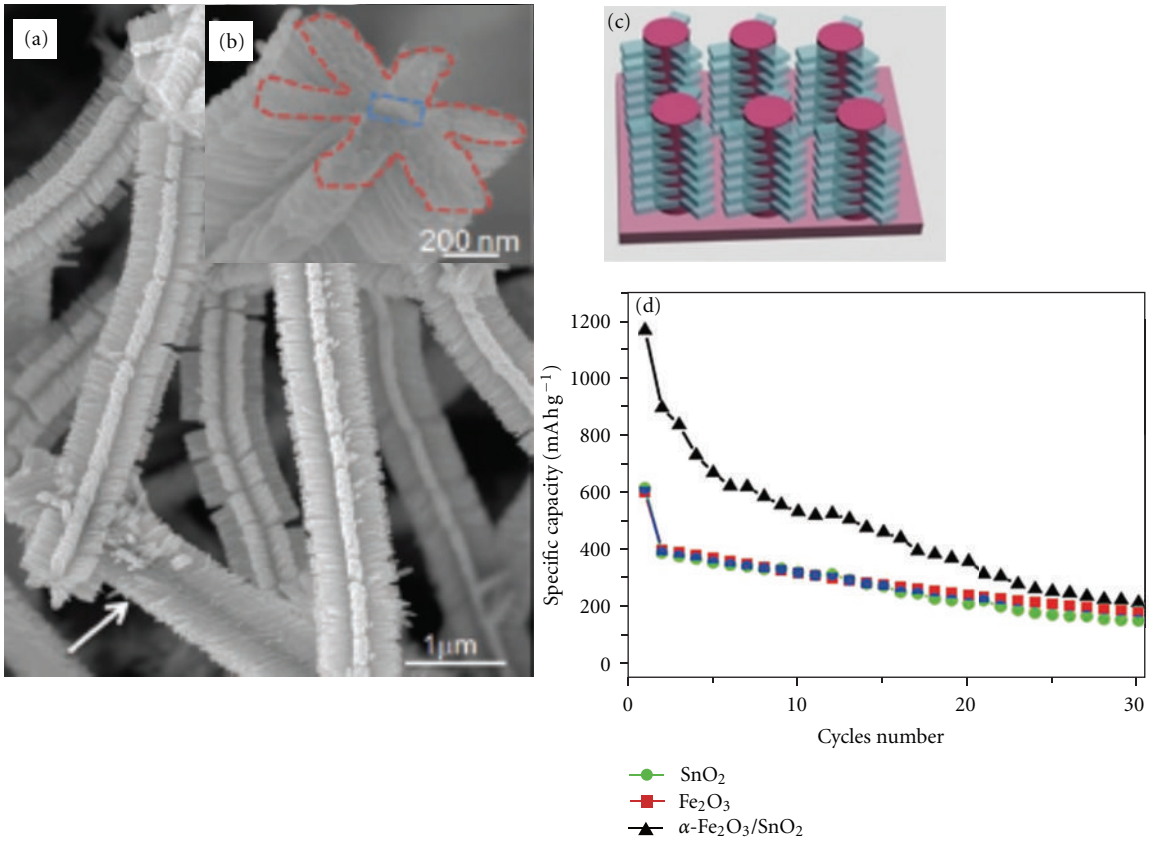

Figure 12: SEM images (a, b) and structural schematic (c) of branched α-Fe_2O_3/SnO_2 nanostructures, (d) cycling performance of α-Fe_2O_3/NRs arrays, pristine SnO_2 NWs, and α-Fe_2O_3/SnO_2 nanostructures at a rate of 1 A g^{-1} [104].

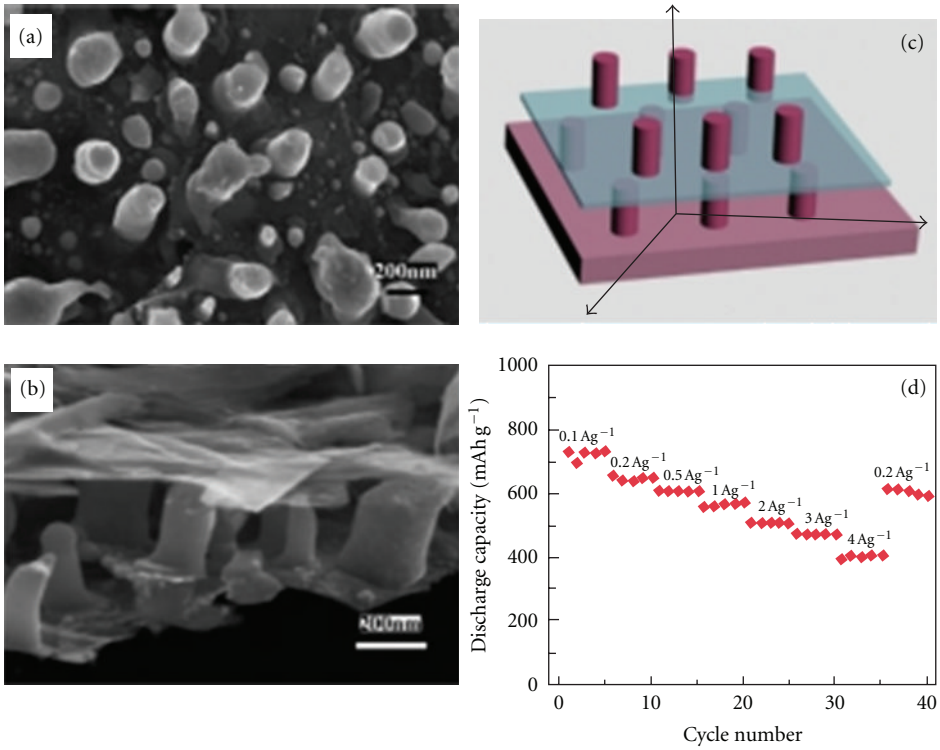

Figure 13: SEM images (a, b), structural schematic (c), and rate cyclability (d) of the graphene/Sn-nanopillar nanostructures [85].

[103] fabricated by Jiang et al. via a hydrothermal method delivered reversible capacities of 690, 572, and 445 mAh g^{-1} at the current density of 1478, 2958, and 5804 mA g^{-1}, respectively. Zhou et al. reported that the branched α-Fe_2O_3/SnO_2 [104] (see Figure 12) prepared by combining a vapor transport deposition and a facile hydrothermal method showed a remarkably improved initial discharge capacity of 1167 mAh g^{-1}, which was about twice the SnO_2 NWs (612 mAh g^{-1}), and α-Fe_2O_3 NRs (598 mAh g^{-1}). The higher capacity of the branched α-Fe_2O_3/SnO_2 is due to that α-Fe_2O_3 branches provide new Li^+ hosts, increase the reversible capacity, and suppress the degradation of the core SnO_2.

4.2.6. Folded Heterogeneous Nanostructure Arrays. Even though complicated, the folded heterogeneous nanostructure arrays are ordinarily composed of multilayered 1D nanostructure arrays embedded between 2D sheets, offering the morphological flexibility to hamper the structural collapse and efficient transport of both Li^+ and electrons and leading to the excellent electrochemical performance [147]. Ji et al. reported that a multilayered graphene/Sn-nanopillar nanostructure (Figure 13), by using the self-assembly and annealing processes, retained a reversible capacity of 501 and 408 mAh g^{-1} at a current density of 1 and 5 A g^{-1} after 35 cycles, respectively, which could be attributed to that both graphene and Sn served as electroactive materials, electronic conductive materials, and mechanically supporting materials [85].

5. Conclusions and Outlook

In conclusion, the recent advances in the design, fabrication, and properties of 3DSNAEs with homogeneous or heterogeneous nanoarchitectured structures for LIBs have been reviewed in detail here. Table 1 illustrates an evaluation of optimizing various electrode materials and suitable strategies to construct 3DSNAEs on various current collector substrates. From an industrial perspective, solution-based growth at low temperature and hydrothermal methods are considered to be most promising for constructing 3DSNAEs with proper electrode materials and proper electrode structures.

Evidently, the nanostructure arrays of 3DSNAEs connected to the conductive collector substrate become mechanically unstable when they are grown excessively long in the axial direction. Besides, the electrochemical performance of 3DSNAEs strongly depends on the physical/chemical properties of interface within the heterogeneous nanoarchitectured structures. Systematic/synergetic combining of the mechanical integrity and electrochemical kinetic properties of 3DSNAEs, therefore, will be required to the development of high-performance LIBs.

It can be seen that a large amount of research has been made in designing homogeneous or heterogeneous nanoarchitectured arrays in 3DSNAEs. On one hand, the hybrid structures among 1D NWs, NRs, and 2D nanosheets increase the specific energy density (especially the area and volumetric energy densities) of electrodes, by making full use of voids within the electrodes, and function simultaneously

as "stabilizers" and "buffers" to the 3DSNAEs with excellent cycling stability. On the other, the heterogeneous components concept opens a promising avenue for designing multifunctional 3DSNAEs by integrating the superiorities of each constituent. Therefore, designing the multifunctional 3DSNAEs with synergic properties by selecting suitable electrode materials and suitable structures is a bright way to address different requirements (high energy density, high conductivity, good mechanical stability, etc.) of superperformance LIBs applied in portable electronic consumer devices, electric vehicles, and large-scale electricity storage.

References

[1] A. S. Aricò, P. Bruce, B. Scrosati, J. M. Tarascon, and W. Van Schalkwijk, "Nanostructured materials for advanced energy conversion and storage devices," *Nature Materials*, vol. 4, no. 5, pp. 366–377, 2005.

[2] M. Armand and J. M. Tarascon, "Building better batteries," *Nature*, vol. 451, no. 7179, pp. 652–657, 2008.

[3] J. B. Goodenough and Y. Kim, "Challenges for rechargeable Li batteries," *Chemistry of Materials*, vol. 22, pp. 587–603, 2009.

[4] J. M. Tarascon and M. Armand, "Issues and challenges facing rechargeable lithium batteries," *Nature*, vol. 414, no. 6861, pp. 359–367, 2001.

[5] Annual Energy Outlook, 2010, http://www.eia.gov/ieo.

[6] F. Cheng, J. Liang, Z. Tao, and J. Chen, "Functional materials for rechargeable batteries," *Advanced Materials*, vol. 23, no. 15, pp. 1695–1715, 2011.

[7] G. Jeong, Y. U. Kim, H. Kim, Y. J. Kim, and H. J. Sohn, "Prospective materials and applications for Li secondary batteries," *Energy and Environmental Science*, vol. 4, no. 6, pp. 1986–2002, 2011.

[8] M. S. Whittingham, "Lithium batteries and cathode materials," *Chemical Reviews*, vol. 104, no. 10, pp. 4271–4301, 2004.

[9] M. Okubo, E. Hosono, J. Kim et al., "Nanosize effect on high-rate Li-ion intercalation in $LiCoO_2$ electrode," *Journal of the American Chemical Society*, vol. 129, no. 23, pp. 7444–7452, 2007.

[10] E. Hosono, T. Kudo, I. Honma, H. Matsuda, and H. Zhou, "Synthesis of single crystalline spinel $LiMn_2O_4$ nanowires for a lithium ion battery with high power density," *Nano Letters*, vol. 9, no. 3, pp. 1045–1051, 2009.

[11] C. S. Johnson, N. Li, C. Lefief, J. T. Vaughey, and M. M. Thackeray, "Synthesis, characterization and electrochemistry of lithium battery electrodes: $xLi_2MnO_{3\cdot(1-x)}LiMn_{0.333}Ni_{0.333}Co_{0.333}O_2$ $(0 \leq x \leq 0.7)$," *Chemistry of Materials*, vol. 20, no. 19, pp. 6095–6106, 2008.

[12] S. Yang, X. Zhou, J. Zhang, and Z. Liu, "Morphology-controlled solvothermal synthesis of $LiFePO_4$ as a cathode material for lithium-ion batteries," *Journal of Materials Chemistry*, vol. 20, no. 37, pp. 8086–8091, 2010.

[13] G. Li, S. Pang, L. Jiang, Z. Guo, and Z. Zhang, "Environmentally friendly chemical route to vanadium oxide single-crystalline nanobelts as a cathode material for lithium-ion batteries," *Journal of Physical Chemistry B*, vol. 110, no. 19, pp. 9383–9386, 2006.

[14] H. K. Song, K. T. Lee, M. G. Kim, L. F. Nazar, and J. Cho, "Recent progress in nanostructured cathode materials for lithium secondary batteries," *Advanced Functional Materials*, vol. 20, no. 22, pp. 3818–3834, 2010.

[15] B. L. Ellis, K. T. Lee, and L. F. Nazar, "Positive electrode materials for Li-Ion and Li-batteries," *Chemistry of Materials*, vol. 22, no. 3, pp. 691–714, 2010.

[16] N. A. Kaskhedikar and J. Maier, "Lithium storage in carbon nanostructures," *Advanced Materials*, vol. 21, no. 25-26, pp. 2664–2680, 2009.

[17] H. Kim, M. Seo, M. H. Park, and J. Cho, "A critical size of silicon nano-anodes for lithium rechargeable batteries," *Angewandte Chemie*, vol. 49, no. 12, pp. 2146–2149, 2010.

[18] J. Hassoun, S. Panero, P. Simon, P. L. Taberna, and B. Scrosati, "High-rate, long-life Ni-Sn nanostructured electrodes for lithium-ion batteries," *Advanced Materials*, vol. 19, no. 12, pp. 1632–1635, 2007.

[19] C. M. Park, J. H. Kim, H. Kim, and H. J. Sohn, "Li-alloy based anode materials for Li secondary batteries," *Chemical Society Reviews*, vol. 39, no. 8, pp. 3115–3141, 2010.

[20] P. Poizot, S. Laruelle, S. Grugeon, L. Dupont, and J. M. Tarascon, "Nano-sized transition-metal oxides as negative-electrode materials for lithium-ion batteries," *Nature*, vol. 407, no. 6803, pp. 496–499, 2000.

[21] I. A. Courtney and J. R. Dahn, "Electrochemical and in situ X-ray diffraction studies of the reaction of lithium with tin oxide composites," *Journal of the Electrochemical Society*, vol. 144, no. 6, pp. 2045–2052, 1997.

[22] I. Exnar, L. Kavan, S. Y. Huang, and M. Grätzel, "Novel 2V rocking-chair lithium battery based on nano-crystalline titanium dioxide," *Journal of Power Sources*, vol. 68, no. 2, pp. 720–722, 1997.

[23] J. Cabana, L. Monconduit, D. Larcher, and M. R. Palacín, "Beyond intercalation-based Li-ion batteries: the state of the art and challenges of electrode materials reacting through conversion reactions," *Advanced Materials*, vol. 22, no. 35, pp. E170–E192, 2010.

[24] L. Ji, Z. Lin, M. Alcoutlabi, and X. Zhang, "Recent developments in nanostructured anode materials for rechargeable lithium-ion batteries," *Energy and Environmental Science*, vol. 4, no. 8, pp. 2682–2689, 2011.

[25] P. G. Bruce, B. Scrosati, and J. M. Tarascon, "Nanomaterials for rechargeable lithium batteries," *Angewandte Chemie*, vol. 47, no. 16, pp. 2930–2946, 2008.

[26] F. Cheng, Z. Tao, J. Liang, and J. Chen, "Template-directed materials for rechargeable lithium-ion batteries," *Chemistry of Materials*, vol. 20, no. 3, pp. 667–681, 2008.

[27] J. W. Long, B. Dunn, D. R. Rolison, and H. S. White, "Three-dimensional battery architectures," *Chemical Reviews*, vol. 104, no. 10, pp. 4463–4492, 2004.

[28] X. W. Lou, L. A. Archer, and Z. Yang, "Hollow micro-/nanostructures: synthesis and applications," *Advanced Materials*, vol. 20, no. 21, pp. 3987–4019, 2008.

[29] Y. K. Sun, S. T. Myung, H. S. Shin, Y. C. Bae, and C. S. Yoon, "Novel core-shell-structured $Li[(Ni_{0.8}Co_{0.2})_{0.8}(Ni_{0.5}Mn_{0.5})_{0.2}]O_2$ via coprecipitation as positive electrode material for lithium secondary batteries," *Journal of Physical Chemistry B*, vol. 110, no. 13, pp. 6810–6815, 2006.

[30] L. W. Su, Y. Jing, and Z. Zhou, "Li ion battery materials with core-shell nanostructures," *Nanoscale*, vol. 3, no. 10, pp. 3967–3983, 2011.

[31] R. Liu, J. Duay, and S. B. Lee, "Heterogeneous nanostructured electrode materials for electrochemical energy storage," *Chemical Communications*, vol. 47, no. 5, pp. 1384–1404, 2011.

[32] D. R. Rolison, J. W. Long, J. C. Lytle et al., "Multifunctional 3D nanoarchitectures for energy storage and conversion," *Chemical Society Reviews*, vol. 38, no. 1, pp. 226–252, 2009.

[33] N. Meethong, H. Y. S. Huang, W. C. Carter, and Y. M. Chiang, "Size-dependent lithium miscibility gap in nanoscale Li 1-xFePO4," *Electrochemical and Solid-State Letters*, vol. 10, no. 5, pp. 134–138, 2007.

[34] L. J. Fu, H. Liu, C. Li et al., "Surface modifications of electrode materials for lithium ion batteries," *Solid State Sciences*, vol. 8, no. 2, pp. 113–128, 2006.

[35] T. Fang, J. G. Duh, and S. R. Sheen, "Improving the electrochemical performance of $LiCoO_2$ cathode by nanocrystalline ZnO coating," *Journal of the Electrochemical Society*, vol. 152, no. 9, pp. A1701–A1706, 2005.

[36] A. I. Hochbaum and P. Yang, "Semiconductor nanowires for energy conversion," *Chemical Reviews*, vol. 110, no. 1, pp. 527–546, 2010.

[37] C. K. Chan, H. Peng, G. Liu et al., "High-performance lithium battery anodes using silicon nanowires," *Nature Nanotechnology*, vol. 3, no. 1, pp. 31–35, 2008.

[38] J. Liu, G. Cao, Z. Yang et al., "Oriented nanostructures for energy conversion and storage.," *ChemSusChem*, vol. 1, no. 8-9, pp. 676–697, 2008.

[39] C. Liu, F. Li, M. Lai-Peng, and H. M. Cheng, "Advanced materials for energy storage," *Advanced Materials*, vol. 22, no. 8, pp. E28–E62, 2010.

[40] J. Jiang, Y. Li, J. Liu, and X. Huang, "Building one-dimensional oxide nanostructure arrays on conductive metal substrates for lithium-ion battery anodes," *Nanoscale*, vol. 3, no. 1, pp. 45–58, 2011.

[41] Z. R. Dai, Z. W. Pan, and Z. L. Wang, "Novel nanostructures of functional oxides synthesized by thermal evaporation," *Advanced Functional Materials*, vol. 13, no. 1, pp. 9–24, 2003.

[42] R. S. Wagner, W. C. Ellis, K. A. Jackson, and S. M. Arnold, "Study of the filamentary growth of silicon crystals from the vapor," *Journal of Applied Physics*, vol. 35, no. 10, pp. 2993–3000, 1964.

[43] A. Sekar, S. H. Kim, A. Umar, and Y. B. Hahn, "Catalyst-free synthesis of ZnO nanowires on Si by oxidation of Zn powders," *Journal of Crystal Growth*, vol. 277, no. 1–4, pp. 471–478, 2005.

[44] J. Yan, A. Sumboja, E. Khoo, and P. S. Lee, "V_2O_5 loaded on SnO_2 nanowires for high rate Li ion batteries," *Advanced Materials*, vol. 23, no. 6, pp. 746–750, 2010.

[45] C. K. Chan, H. Peng, R. D. Twesten, K. Jarausch, X. F. Zhang, and Y. Cui, "Fast, completely reversible Li insertion in vanadium pentoxide nanoribbons," *Nano Letters*, vol. 7, no. 2, pp. 490–495, 2007.

[46] M. D. Fleischauer, J. Li, and M. J. Brett, "Columnar thin films for three-dimensional microbatteries," *Journal of the Electrochemical Society*, vol. 156, no. 1, pp. A33–A36, 2009.

[47] Y. D. Ko, J. G. Kang, J. G. Park, S. Lee, and D. W. Kim, "Self-supported SnO_2 nanowire electrodes for high-power lithium-ion batteries," *Nanotechnology*, vol. 20, no. 45, Article ID 455701, 2009.

[48] L. Zheng, Y. Xu, D. Jin, and Y. Xie, "Well-aligned molybdenum oxide nanorods on metal substrates: solution-based synthesis and their electrochemical capacitor application," *Journal of Materials Chemistry*, vol. 20, no. 34, pp. 7135–7143, 2010.

[49] Y. Wang, H. Xia, L. Lu, and J. Lin, "Excellent performance in lithium-ion battery anodes: rational synthesis of $Co(CO_3)_{0.5}(OH)_{0.11}H_2O$ nanobelt array and its conversion into mesoporous and single-crystal Co_3O_4," *ACS Nano*, vol. 4, no. 3, pp. 1425–1432, 2010.

[50] Y. Song, S. Qin, Y. Zhang, W. Gao, and J. Liu, "Large-scale porous hematite nanorod arrays: direct growth on titanium foil and reversible lithium storage," *Journal of Physical Chemistry C*, vol. 114, no. 49, pp. 21158–21164, 2010.

[51] L. E. Greene, M. Law, D. H. Tan et al., "General route to vertical ZnO nanowire arrays using textured ZnO seeds," *Nano Letters*, vol. 5, no. 7, pp. 1231–1236, 2005.

[52] H. Yu, Z. Zhang, M. Han, X. Hao, and F. Zhu, "A general low-temperature route for large-scale fabrication of highly oriented ZnO nanorod/nanotube arrays," *Journal of the American Chemical Society*, vol. 127, no. 8, pp. 2378–2379, 2005.

[53] L. E. Greene, M. Law, J. Goldberger et al., "Low-temperature wafer-scale production of ZnO nanowire arrays," *Angewandte Chemie*, vol. 42, no. 26, pp. 3031–3034, 2003.

[54] Y. Li, B. Tan, and Y. Wu, "Mesoporous Co_3O_4 nanowire arrays for lithium ion batteries with high capacity and rate capability," *Nano Letters*, vol. 8, no. 1, pp. 265–270, 2008.

[55] Z. Huang, N. Geyer, P. Werner, J. De Boor, and U. Gösele, "Metal-assisted chemical etching of silicon: a review," *Advanced Materials*, vol. 23, no. 2, pp. 285–308, 2011.

[56] C. M. Hsu, S. T. Connor, M. X. Tang, and Y. Cui, "Wafer-scale silicon nanopillars and nanocones by Langmuir-Blodgett assembly and etching," *Applied Physics Letters*, vol. 93, no. 13, Article ID 133109, 2008.

[57] W. Zhang, X. Wen, and S. Yang, "Controlled reactions on a copper surface: synthesis and characterization of nanostructured copper compound films," *Inorganic Chemistry*, vol. 42, no. 16, pp. 5005–5014, 2003.

[58] J. Y. Xiang, J. P. Tu, X. H. Huang, and Y. Z. Yang, "A comparison of anodically grown CuO nanotube film and Cu_2O film as anodes for lithium ion batteries," *Journal of Solid State Electrochemistry*, vol. 12, no. 7-8, pp. 941–945, 2008.

[59] F. S. Ke, L. Huang, G. Z. Wei et al., "One-step fabrication of CuO nanoribbons array electrode and its excellent lithium storage performance," *Electrochimica Acta*, vol. 54, no. 24, pp. 5825–5829, 2009.

[60] C. H. Lai, K. W. Huang, J. H. Cheng et al., "Oriented growth of large-scale nickel sulfide nanowire arrays via a general solution route for lithium-ion battery cathode applications," *Journal of Materials Chemistry*, vol. 19, no. 39, pp. 7277–7283, 2009.

[61] F. Fabregat-Santiago, E. M. Barea, J. Bisquert, G. K. Mor, K. Shankar, and C. A. Grimes, "High carrier density and capacitance in TiO_2 nanotube arrays induced by electrochemical doping," *Journal of the American Chemical Society*, vol. 130, no. 34, pp. 11312–11316, 2008.

[62] G. F. Ortiz, I. Hanzu, T. Djenizian, P. Lavela, J. L. Tirado, and P. Knauth, "Alternative Li-ion battery electrode based on self-organized titania nanotubes," *Chemistry of Materials*, vol. 21, no. 1, pp. 63–67, 2009.

[63] X. Chen, N. Q. Zhang, and K. N. Sun, "A vapor-phase corrosion strategy to hierarchically mesoporous nanosheet-assembled gearlike pillar arrays for super-performance lithium storage," *The Journal of Physical Chemistry C*, vol. 116, no. 40, pp. 21224–21231.

[64] X. Chen, N. Q. Zhang, and K. N. Sun, "Facile fabrication of CuO mesoporous nanosheet cluster array electrodes with super lithium-storage properties," *Journal of Materials Chemistry*, vol. 22, no. 27, pp. 13637–13642, 2012.

[65] P. L. Taberna, S. Mitra, P. Poizot, P. Simon, and J. M. Tarascon, "High rate capabilities Fe_3O_4-based Cu nano-architectured electrodes for lithium-ion battery applications," *Nature Materials*, vol. 5, no. 7, pp. 567–573, 2006.

[66] J. H. Kim, T. Ayalasomayajula, V. Gona, and D. Choi, "Fabrication and electrochemical characterization of a vertical array of MnO_2 nanowires grown on silicon substrates as a cathode material for lithium rechargeable batteries," *Journal of Power Sources*, vol. 183, no. 1, pp. 366–369, 2008.

[67] Y. S. Kim, H. J. Ahn, S. H. Nam, S. H. Lee, H. S. Shim, and W. B. Kim, "Honeycomb pattern array of vertically standing core-shell nanorods: its application to Li energy electrodes," *Applied Physics Letters*, vol. 93, no. 10, Article ID 103104, 2008.

[68] K. Takahashi, Y. Wang, K. Lee, and G. Cao, "Fabrication and Li^+-intercalation properties of V_2O_5-TiO_2 composite nanorod arrays," *Applied Physics A*, vol. 82, no. 1, pp. 27–31, 2006.

[69] Y. Wang, K. Takahashi, H. Shang, and G. Cao, "Synthesis and electrochemical properties of vanadium pentoxide nanotube arrays," *Journal of Physical Chemistry B*, vol. 109, no. 8, pp. 3085–3088, 2005.

[70] M. M. Shaijumon, E. Perre, B. Daffos, P. L. Taberna, J. M. Tarascon, and P. Simon, "Nanoarchitectured 3D cathodes for Li-ion microbatteries," *Advanced Materials*, vol. 22, no. 44, pp. 4978–4981, 2010.

[71] Y. Wang and G. Cao, "Synthesis and electrochemical properties of $InVO_4$ nanotube arrays," *Journal of Materials Chemistry*, vol. 17, no. 9, pp. 894–899, 2007.

[72] I. Lahiri, S. W. Oh, J. Y. Hwang et al., "High capacity and excellent stability of lithium ion battery anode using interface-controlled binder-free multiwall carbon nanotubes grown on copper," *ACS Nano*, vol. 4, no. 6, pp. 3440–3446, 2010.

[73] R. Teki, R. Krishnan, T. C. Parker, T. M. Lu, P. N. Kumta, and N. Koratkar, "Nanostructured silicon anodes for lithium Ion rechargeable batteries," *Small*, vol. 5, no. 20, pp. 2236–2242, 2009.

[74] L. Bazin, S. Mitra, P. L. Taberna et al., "High rate capability pure Sn-based nano-architectured electrode assembly for rechargeable lithium batteries," *Journal of Power Sources*, vol. 188, no. 2, pp. 578–582, 2009.

[75] A. Finke, P. Poizot, C. Guéry et al., "Electrochemical method for direct deposition of nanometric bismuth and its electrochemical properties vs Li," *Electrochemical and Solid-State Letters*, vol. 11, no. 3, pp. E5–E9, 2008.

[76] Z. Wang, F. Su, S. Madhavi, and X. W. Lou, "CuO nanostructures supported on Cu substrate as integrated electrodes for highly reversible lithium storage," *Nanoscale*, vol. 3, no. 4, pp. 1618–1623, 2011.

[77] H. Wang, Q. Pan, Y. Cheng, J. Zhao, and G. Yin, "Evaluation of ZnO nanorod arrays with dandelion-like morphology as negative electrodes for lithium-ion batteries," *Electrochimica Acta*, vol. 54, no. 10, pp. 2851–2855, 2009.

[78] Q. Pan, L. Qin, J. Liu, and H. Wang, "Flower-like ZnO-NiO-C films with high reversible capacity and rate capability for lithium-ion batteries," *Electrochimica Acta*, vol. 55, no. 20, pp. 5780–5785, 2010.

[79] G. Ferrara, L. Damen, C. Arbizzani et al., "SnCo nanowire array as negative electrode for lithium-ion batteries," *Journal of Power Sources*, vol. 196, no. 3, pp. 1469–1473, 2011.

[80] M. Tian, W. Wang, S. H. Lee et al., "Enhancing Ni-Sn nanowire lithium-ion anode performance by tailoring active/inactive material interfaces," *Journal of Power Sources*, vol. 196, no. 23, pp. 10207–10212, 2011.

[81] M. Tian, W. Wang, Y. J. Wei, and R. G. Yang, "Stable high areal capacity lithium-ion battery anodes based on three-dimensional Ni-Sn nanowire networks," *Journal of Power Sources*, vol. 211, no. 23, pp. 46–51, 2012.

[82] J. Z. Wang, N. Du, H. Zhang et al., "Cu-$Si_{1-x}Ge_x$Core-Shell nanowire arrays as three-dimensional electrodes for high-rate capability lithium-ion batteries," *Journal of Power Sources*, vol. 208, no. 15, pp. 434–439, 2012.

[83] C. H. Lai, K. W. Huang, J. H. Cheng, C. Y. Lee, B. J. Hwang, and L. J. Chen, "Direct growth of high-rate capability and high capacity copper sulfide nanowire array cathodes for lithium-ion batteries," *Journal of Materials Chemistry*, vol. 20, no. 32, pp. 6638–6645, 2010.

[84] C. Villevieille, F. Robert, P. L. Taberna, L. Bazin, P. Simon, and L. Monconduit, "The good reactivity of lithium with nanostructured copper phosphide," *Journal of Materials Chemistry*, vol. 18, no. 48, pp. 5956–5960, 2008.

[85] L. W. Ji, Z. K. Tan, T. Kuykendall et al., "Multilayer nanoassembly of Sn-nanopillar arrays sandiwiched between graphene layers for high-capacity lithium storage," *Energy & Environmental Science*, vol. 4, no. 9, pp. 3611–3616, 2011.

[86] M. S. Wu, P. C. J. Chiang, J. T. Lee, and J. C. Lin, "Synthesis of manganese oxide electrodes with interconnected nanowire structure as an anode material for rechargeable lithium ion batteries," *Journal of Physical Chemistry B*, vol. 109, no. 49, pp. 23279–23284, 2005.

[87] Y. Fan, H. Shao, J. Wang, L. Liu, J. Zhang, and C. Cao, "Synthesis of foam-like freestanding Co_3O_4 nanosheets with enhanced electrochemical activities," *Chemical Communications*, vol. 47, no. 12, pp. 3469–3471, 2011.

[88] J. Liu, Y. Li, X. Huang et al., "Direct growth of SnO_2 nanorod array electrodes for lithium-ion batteries," *Journal of Materials Chemistry*, vol. 19, no. 13, pp. 1859–1864, 2009.

[89] J. Liu, Y. Li, H. Fan et al., "Iron oxide-based nanotube arrays derived from sacrificial template-accelerated hydrolysis: large-area design and reversible lithium storage," *Chemistry of Materials*, vol. 22, no. 1, pp. 212–217, 2010.

[90] J. Liu, Y. Li, R. Ding et al., "Carbon/ZnO nanorod array electrode with significantly improved lithium storage capability," *Journal of Physical Chemistry C*, vol. 113, no. 13, pp. 5336–5339, 2009.

[91] N. Zhao, G. Wang, Y. Huang, B. Wang, B. Yao, and Y. Wu, "Preparation of nanowire arrays of amorphous carbon nanotube-coated single crystal SnO_2," *Chemistry of Materials*, vol. 20, no. 8, pp. 2612–2614, 2008.

[92] A. L. M. Reddy, M. M. Shaijumon, S. R. Gowda, and P. M. Ajayan, "Coaxial MnO_2/carbon nanotube array electrodes for high-performance lithium batteries," *Nano Letters*, vol. 9, no. 3, pp. 1002–1006, 2009.

[93] G. Ferrara, C. Arbizzani, and L. Damen, "High-performing SnCo nanowire electrodes as anodes for lithium-ion batteries," *Journal of Power Sources*, vol. 211, pp. 103–107, 2012.

[94] C. Masarapu, V. Subramanian, H. Zhu, and B. Wei, "Long-cycle electrochemical behavior of multiwall carbon nanotubes synthesized on stainless steel in Li ion batteries," *Advanced Functional Materials*, vol. 19, no. 7, pp. 1008–1014, 2009.

[95] C. K. Chan, X. F. Zhang, and Y. Cui, "High capacity Li ion battery anodes using Ge nanowires," *Nano Letters*, vol. 8, no. 1, pp. 307–309, 2008.

[96] L. Hu, H. Wu, S. S. Hong et al., "Si nanoparticle-decorated Si nanowire networks for Li-ion battery anodes," *Chemical Communications*, vol. 47, no. 1, pp. 367–369, 2011.

[97] L. F. Cui, R. Ruffo, C. K. Chan, H. Peng, and Y. Cui, "Crystalline-amorphous core-shell silicon nanowires for high capacity and high current battery electrodes," *Nano Letters*, vol. 9, no. 1, pp. 491–495, 2009.

[98] A. Gohier, B. Laïk, J. P. Pereira-Ramos et al., "Influence of the diameter distribution on the rate capability of silicon nanowires for lithium-ion batteries," *Journal of Power Sources*, vol. 203, pp. 135–139, 2012.

[99] N. Liu, L. B. Hu, M. T. McDowell et al., "Prelithiated silicon nanowires as an anode for lithium ion batteries," *ACS Nano*, vol. 5, no. 8, pp. 6487–6493, 2011.

[100] L. F. Cui, L. Hu, J. W. Choi, and Y. Cui, "Light-weight free-standing carbon nanotube-silicon films for anodes of lithium ion batteries," *ACS Nano*, vol. 4, no. 7, pp. 3671–3678, 2010.

[101] H. Chen, Y. Xiao, L. Wang, and Y. Yang, "Silicon nanowires coated with copper layer as anode materials for lithium-ion batteries," *Journal of Power Sources*, vol. 196, no. 16, pp. 6657–6662, 2011.

[102] K. S. Park, J. G. Kang, Y. J. Choi, S. Lee, D. W. Kim, and J. G. Park, "Long-term, high-rate lithium storage capabilities of TiO_2 nanostructured electrodes using 3D self-supported indium tin oxide conducting nanowire arrays," *Energy and Environmental Science*, vol. 4, no. 5, pp. 1796–1801, 2011.

[103] J. Jiang, J. H. Zhu, Y. M. Feng et al., "A novel evolution strategy to fabricate a 3D hierarchical interconnected core-shell Ni/MnO_2 hybrid for Li-ion batteries," *Chemical Communications*, vol. 48, no. 60, pp. 7471–7473, 2012.

[104] W. Zhou, C. Cheng, J. Liu et al., "Epitaxial growth of branched α-Fe_2O_3/SnO_2 nano-heterostructures with improved lithium-ion battery performance," *Advanced Functional Materials*, vol. 21, no. 13, pp. 2439–2445, 2011.

[105] S. Luo, K. Wang, J. P. Wang et al., "Binder-free $LiCoO_2$/carbon nanotube cathodes for high-performance lithium ion batteries," *Advanced Materials*, vol. 24, no. 17, pp. 2294–2298, 2012.

[106] J. J. Schneider, J. Khanderi, A. Popp et al., "Hybrid architectures from 3D aligned arrays of multiwall carbon nanotubes and nanoparticulate $LiCoPO_4$: synthesis, properties and evaluation of their electrochemical performance as cathode materials in lithium ion batteries," *European Journal of Inorganic Chemistry*, vol. 211, no. 28, pp. 4349–4359, 2011.

[107] L. Dimesso, C. Förster, W. Jaegermann et al., "Developments in nanostructured $LiMPO_4$(M= Fe, Co, Ni, Mn) composites based on three dimensional carbon architecture," *Chemical Society Reviews*, vol. 41, no. 15, pp. 5068–5080, 2012.

[108] Y. Wang, H. J. Zhang, W. X. Lim, J. Y. Lin, and C. C. Wong, "Designed strategy to fabricate a patterned V_2O_5 nanobelt array as a superior electrode for Li-ion batteries," *Journal of Materials Chemistry*, vol. 21, no. 7, pp. 2362–2368, 2011.

[109] G. Du, Z. Guo, P. Zhang et al., "SnO_2 nanocrystals on self-organized TiO_2 nanotube array as three-dimensional electrode for lithium ion microbatteries," *Journal of Materials Chemistry*, vol. 20, no. 27, pp. 5689–5694, 2010.

[110] M. C. Qiu, L. W. Yang, X. Qi, J. Li, and J. X. Zhong, "Fabrication of ordered NiO coated Si nanowire array films as electrodes for a high performance lithium ion battery," *ACS Applied Materials and Interfaces*, vol. 2, no. 12, pp. 3614–3618, 2010.

[111] D. Liu, Q. Zhang, P. Xiao et al., "Hydrous manganese dioxide nanowall arrays growth and their Li+ ions intercalation electrochemical properties," *Chemistry of Materials*, vol. 20, no. 4, pp. 1376–1380, 2008.

[112] Y. H. Lee, I. C. Leu, C. L. Liao et al., "Fabrication and characterization of Cu_2O nanorod arrays and their electrochemical performance in Li-ion batteries," *Electrochemical and Solid-State Letters*, vol. 9, no. 4, pp. A207–A210, 2006.

[113] J. H. Kim, S. Khanal, M. Islam, A. Khatri, and D. Choi, "Electrochemical characterization of vertical arrays of tin nanowires grown on silicon substrates as anode materials for lithium rechargeable microbatteries," *Electrochemistry Communications*, vol. 10, no. 11, pp. 1688–1690, 2008.

[114] S. S. Zhang and T. R. Jow, "Aluminum corrosion in electrolyte of Li-ion battery," *Journal of Power Sources*, vol. 109, no. 2, pp. 458–464, 2002.

[115] S. T. Myung, Y. Hitoshi, and Y. K. Sun, "Electrochemical behavior and passivation of current collectors in lithium-ion batteries," *Journal of Materials Chemistry*, vol. 21, no. 27, pp. 9891–9911, 2011.

[116] K. Takahashi, S. J. Limmer, Y. Wang, and G. Cao, "Synthesis and electrochemical properties of single-crystal V_2O_5 nanorod arrays by template-based electrodeposition," *Journal of Physical Chemistry B*, vol. 108, no. 28, pp. 9795–9800, 2004.

[117] K. Takahashi, S. J. Limmer, Y. Wang, and G. Cao, "Growth and electrochemical properties of single-crystalline V_2O_5 nanorod arrays," *Japanese Journal of Applied Physics Part 1*, vol. 44, no. 1 B, pp. 662–668, 2005.

[118] K. Takahashi, Y. Wang, and G. Z. Cao, "Ni-$V_2O_5\cdot$ nH_2O core-shell nanocable arrays for enhanced electrochemical intercalation," *The Journal of Physical Chemistry B*, vol. 109, no. 1, pp. 48–51, 2005.

[119] E. Perre, L. Nyholm, T. Gustafsson, P. L. Taberna, P. Simon, and K. Edström, "Direct electrodeposition of aluminium nano-rods," *Electrochemistry Communications*, vol. 10, no. 10, pp. 1467–1470, 2008.

[120] G. Oltean, L. Nyholm, and K. Edström, "Galvanostatic electrodeposition of aluminium nano-rods for Li-ion three-dimensional micro-battery current collectors," *Electrochimica Acta*, vol. 56, no. 9, pp. 3203–3208, 2011.

[121] S. Zhang, Z. Du, R. Lin et al., "Nickel nanocone-array supported silicon anode for high-performance lithium-ion batteries," *Advanced Materials*, vol. 22, no. 47, pp. 5378–5382, 2010.

[122] H. Duan, J. Gnanaraj, X. Chen, B. Li, and J. Liang, "Fabrication and characterization of Fe_3O_4-based Cu nanostructured electrode for Li-ion battery," *Journal of Power Sources*, vol. 185, no. 1, pp. 512–518, 2008.

[123] H. Duan, J. Gnanaraj, and J. Liang, "Synthesis and rate performance of Fe_3O_4-based Cu nanostructured electrodes for Li ion batteries," *Journal of Power Sources*, vol. 196, no. 10, pp. 4779–4784, 2011.

[124] D. D. Jiang, H. Y. Tian, C. C. Qiu et al., "Electrodeposition and characterization of assembly of Sn on Cu nanorods for Li-ion microbattery application," *Journal of Solid State Electrochemistry*, vol. 15, no. 11-12, pp. 2639–2644, 2011.

[125] H. Lee, J. J. Cho, J. Kim, and H. J. Kim, "Comparison of voltammetric responses over the cathodic region in $LiPF_6$ and LiBETI with and without HF," *Journal of the Electrochemical Society*, vol. 152, no. 6, pp. A1193–A1198, 2005.

[126] X. Ji, X. Huang, J. Liu et al., "Carbon-coated SnO_2 nanorod array for lithium-ion battery anode material," *Nanoscale Research Letters*, vol. 5, no. 3, pp. 649–653, 2010.

[127] C. Iwakura, Y. Fukumoto, H. Inoue et al., "Electrochemical characterization of various metal foils as a current collector of positive electrode for rechargeable lithium batteries," *Journal of Power Sources*, vol. 68, no. 2, pp. 301–303, 1997.

[128] Z. Wei, Z. Liu, R. Jiang, C. Bian, T. Huang, and A. Yu, "TiO_2 nanotube array film prepared by anodization as anode material for lithium ion batteries," *Journal of Solid State Electrochemistry*, vol. 14, no. 6, pp. 1045–1050, 2010.

[129] D. Liu, P. Xiao, Y. Zhang et al., "TiO_2 nanotube arrays annealed in N_2 for efficient lithium-ion intercalation," *Journal of Physical Chemistry C*, vol. 112, no. 30, pp. 11175–11180, 2008.

[130] D. Liu, Y. Zhang, P. Xiao et al., "TiO_2 nanotube arrays annealed in CO exhibiting high performance for lithium ion intercalation," *Electrochimica Acta*, vol. 54, no. 27, pp. 6816–6820, 2009.

[131] D. Liu, B. B. Garcia, Q. Zhang et al., "Mesoporous hydrous manganese dioxide nanowall arrays with large lithium ion energy storage capacities," *Advanced Functional Materials*, vol. 19, no. 7, pp. 1015–1023, 2009.

[132] K. Kang, H. S. Lee, D. W. Han et al., "Maximum Li storage in Si nanowires for the high capacity three-dimensional Li-ion battery," *Applied Physics Letters*, vol. 96, no. 5, Article ID 053110, 2010.

[133] H. Wang, Q. Pan, J. Zhao, G. Yin, and P. Zuo, "Fabrication of CuO film with network-like architectures through solution-immersion and their application in lithium ion batteries," *Journal of Power Sources*, vol. 167, no. 1, pp. 206–211, 2007.

[134] Q. Pan, H. Jin, H. Wang, and G. Yin, "Flower-like CuO film-electrode for lithium ion batteries and the effect of surface morphology on electrochemical performance," *Electrochimica Acta*, vol. 53, no. 2, pp. 951–956, 2007.

[135] X. Chen, N. Q. Zhang, and K. N. Sun, "Facile fabrication of CuO 1D pine-needle-like arrays for super-rate lithium storage," *Journal of Materials Chemistry*, vol. 22, no. 30, pp. 15080–15084, 2012.

[136] W. X. Zhang, M. Li, Q. Wang et al., "Hierarchical self-assembly of microscale cog-like superstructures for enhanced performance in lithium-ion batteries," *Advanced Functional Materials*, vol. 21, no. 8, pp. 3516–3523, 2011.

[137] W. Q. Zeng, F. P. Zheng, R. Z. Li et al., "Template synthesis of SnO_2/α-Fe_2O_3 nanotube array for 3D lithium ion battery anode with large areal capacity," *Nanoscale*, vol. 4, no. 8, pp. 2760–2765, 2012.

[138] F. F. Cao, J. W. Deng, S. Xin et al., "Cu-Si nanocable arrays as high-rate anode materials for lithium-ion batteries," *Advanced Materials*, vol. 23, no. 38, pp. 4415–4420, 2011.

[139] X. Chen, K. Gerasopoulos, J. Guo et al., "A patterned 3D silicon anode fabricated by electrodeposition on a virus-structured current collector," *Advanced Functional Materials*, vol. 21, no. 2, pp. 380–387, 2011.

[140] L. B. Hu, H. Wu, Y. F. Gao et al., "Silicon-carbon nanotube coaxial sponge as Li-ion anodes with high areal Capacity," *Advanced Energy Materials*, vol. 1, no. 4, pp. 523–527, 2011.

[141] G. F. Ortiz, I. Hanzu, P. Lavela, P. Knauth, J. L. Tirado, and T. Djenizian, "Nanoarchitectured TiO_2/SnO: a future negative electrode for high power density Li-Ion microbatteries," *Chemistry of Materials*, vol. 22, no. 5, pp. 1926–1932, 2010.

[142] G. F. Ortiz, I. Hanzu, P. Lavela, J. L. Tirado, P. Knauth, and T. Djenizian, "A novel architectured negative electrode based on titania nanotube and iron oxide nanowire composites for Li-ion microbatteries," *Journal of Materials Chemistry*, vol. 20, no. 20, pp. 4041–4046, 2010.

[143] H. Cheng, Z. G. Lu, J. Q. Deng, C. Y. Chung, K. Zhang, and Y. Y. Li, "A facile method to improve the high rate capability of Co_3O_4 nanowire array electrodes," *Nano Research*, vol. 3, no. 12, pp. 895–901, 2010.

[144] W. Wang, R. Epur, and P. N. Kumta, "Vertically aligned silicon/carbon nanotube (VASCNT) arrays: hierarchical anodes for lithium-ion battery," *Electrochemistry Communications*, vol. 13, no. 5, pp. 429–432, 2011.

[145] W. Wang and P. N. Kumta, "Nanostructured hybrid silicon/carbon nanotube heterostructures: reversible high-capacity lithium-ion anodes," *ACS Nano*, vol. 4, no. 4, pp. 2233–2241, 2010.

[146] A. Gohier, B. Laïk, K. H. Kim et al., "High rate capacity silicon decorated vertically aligned carbon nanotubes for Li-ion batteries," *Advanced Materials*, vol. 24, no. 19, pp. 2592–2597, 2012.

[147] T. I. Lee, J. P. Jeagal, J. H. Choi et al., "Binder-free and full electrical-addressing free-standing nanosheets with carbon nanotube fabrics for electrochemical applications," *Advanced Materials*, vol. 23, no. 40, pp. 4711–4715, 2011.